Two FEM-BEM methods for the numerical solution of 2D transient elastodynamics problems in unbounded domains

Two FEM-BEM methods for the numerical solution of 2D transient elastodynamics problems in unbounded domains

S. Falletta[a,*], G. Monegato[a], L. Scuderi[a]

[a] *Dipartimento di Scienze Matematiche "G.L. Lagrange", Dipartimento di Eccellenza 2018-2022*
Politecnico di Torino
Corso Duca degli Abruzzi 24, 10129, Torino, Italia

Abstract

We consider wave propagation problems in 2D unbounded isotropic homogeneous elastic media, with rigid boundary conditions. For their solution, we propose and compare two alternative numerical approaches, both obtained by coupling the problem differential equation with the associated space-time boundary integral equation. The latter is defined on an artificial boundary, chosen to surround the (bounded) exterior computational domain of interest. The integral equation defines a boundary condition which is non reflecting for incoming and also for outgoing waves.

In both approaches, the differential equations are discretized by applying a finite element method, while the discretization of the integral equation is obtained by coupling a time convolution quadrature with a space collocation boundary element method. The construction of the two approaches is described and discussed. Some numerical tests are also presented.

Keywords: Elastic wave propagation, finite element method, boundary element method, convolution quadrature, collocation method.

1. Introduction

We consider elastic wave propagation problems in 2D unbounded domains, exterior to bounded obstacles, with Dirichlet boundary conditions prescribed on the contour of them. We assume that the propagation medium is isotropic and homogeneous. For their solution by means of Boundary Element Methods (BEMs), various numerical approaches have been proposed; among them we mention those reformulated in the frequency domain using the Laplace or Fourier transforms, and those defined by their space-time Boundary Integral Equation (BIE) representation. Concerning these latter, the first numerical strategies were based on the coupling of a time-marching (quadrature) rule with a boundary element spatial discretization (see [15],[17]); later, the time integration has been successfully performed by the convolution quadrature due to Ch. Lubich [12] (see, for example, [16, 11, 9, 14]).

In [8] we solved the above mentioned exterior elastodynamics problems by two alternative BEM approaches. In the first one, a standard BEM is applied to the classical differential equation of elastodynamics, while in the second one, a new BEM has been proposed for the corresponding couple of scalar wave equations, in terms of the P- and S-waves, obtained after performing the displacement Helmholtz decomposition of the original PDE. In each of these two BEM approaches, the discretization of their space-time BIE representations was performed by coupling a Lubich time Convolution Quadrature (CQ) [12] with a classical space collocation method (see [7, 6]).

It is well known that the reconstruction of the vector field of the original PDE at points of the exterior domain entails the post processing evaluation of boundary integrals which involve the computed boundary densities. This procedure may be inefficient, especially when the solution

*Corresponding author.
Email addresses: silvia.falletta@polito.it (S. Falletta), giovanni.monegato@polito.it (G. Monegato), letizia.scuderi@polito.it (L. Scuderi)

has to be evaluated in an entire region surrounding the physical obstacle and the geometry of the boundary is not a simple one. This is also the case because in its vicinity the boundary integrals have near singularities, whose non-trivial evaluation must be suitably performed.

As an alternative approach to overcome this drawback, in this paper we propose a FEM-BEM coupling strategy. In particular, we consider the same two equivalent representations of our transient problem, and the same BIE formulations and discretizations. However, the BIE is now used as an additional non-reflecting boundary condition to be imposed on an artificial boundary surrounding the computational domain of interest. The new formulations are then solved by applying a FEM in the interior domain and the BEM on the artificial boundary.

The FEM-BEM couplings, and their corresponding linear systems to be solved, are described in Sections 2.1.2–2.1.3 and 2.2.2–2.2.3. In Section 3, to test and compare the two alternative numerical approaches that we have proposed to solve our elastodynamics problem, we have applied them to three different problems. From the results we have obtained, some conclusions are then drawn in Section 4.

2. The model problem

Let $\Omega^i \subset \mathbb{R}^2$ be an open, bounded and rigid domain, whose boundary Γ is assumed to be closed and smooth. We aim at studying the propagation of elastic waves in the homogeneous isotropic elastic medium $\Omega^e := \mathbb{R}^2 \backslash \overline{\Omega^i}$, caused by a body force $\mathbf{f}$, with initial conditions $\mathbf{u}_0, \mathbf{z}_0$ and a Dirichlet datum $\mathbf{g}$. Assuming small variations of the displacement field $\mathbf{u}^e(\mathbf{x},t) = (\mathrm{u}_1^e(\mathbf{x},t), \mathrm{u}_2^e(\mathbf{x},t))$, $\mathbf{x} = (x_1, x_2)$, this latter is uniquely defined by the following system:

$$\begin{cases} \rho \dfrac{\partial^2 \mathbf{u}^e}{\partial t^2}(\mathbf{x},t) - (\lambda+\mu)\nabla(\operatorname{div}\mathbf{u}^e)(\mathbf{x},t) - \mu\,\nabla^2\mathbf{u}^e(\mathbf{x},t) & = \mathbf{f}(\mathbf{x},t) \quad (\mathbf{x},t) \in \Omega^e \times (0,T] \\ \mathbf{u}^e(\mathbf{x},t) & = \mathbf{g}(\mathbf{x},t) \quad (\mathbf{x},t) \in \Gamma \times (0,T] \\ \mathbf{u}^e(\mathbf{x},0) & = \mathbf{u}_0(\mathbf{x}) \quad \mathbf{x} \in \Omega^e \\ \mathbf{u}_t^e(\mathbf{x},0) & = \mathbf{z}_0(\mathbf{x}) \quad \mathbf{x} \in \Omega^e, \end{cases} \tag{1}$$

where $\rho > 0$ is the constant material density, $\lambda > 0$ and $\mu > 0$ are the Lamé constants.

As often occurs in practical applications, we assume that the initial condition $\mathbf{u}_0$, the initial velocity $\mathbf{z}_0$ and the source term $\mathbf{f}$ are either trivial or have local supports. Aiming to determine the solution $\mathbf{u}^e$ of the above problem in a bounded subregion of Ω^e, surrounding the physical domain Ω^i, we truncate the infinite domain Ω^e by introducing an artificial smooth boundary $\mathcal{B}$. This boundary divides Ω^e into two open sub-domains: a finite computational domain Ω, which is bounded internally by Γ and externally by $\mathcal{B}$, and an infinite residual domain $\mathcal{D}$ (see Figure 1). Further, we denote by $\mathbf{n}$ and $\mathbf{n}_\mathcal{D}$ the unit normal vectors on $\mathcal{B}$ pointing outside Ω and inside $\mathcal{D}$, respectively (recall that $\mathbf{n} = -\mathbf{n}_\mathcal{D}$).

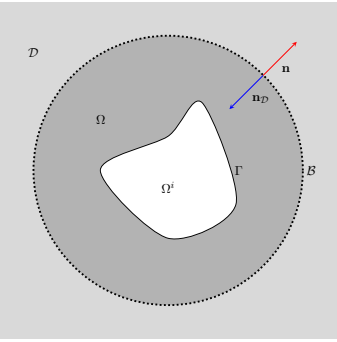

Figure 1: Model problem setting.

To obtain a well posed problem in Ω, we impose a Time Domain Non Reflecting Boundary Condition (TD-NRBC) on $\mathcal{B}$, by using a direct boundary integral equation. The latter is defined by means of suitable boundary operators which involve the fundamental solutions of the elastodynamic equation.

In the following sections we describe the approach we propose, which consists in the coupling of a finite element method for the interior computational domain with a boundary element one for the discretization of the TD-NRBC. We apply such an approach to two formulations of the elastodynamic problem: the first one is defined by the standard vector equation (see Problem (1)); the second one consists of a couple of scalar wave equations obtained by performing the classical Helmholtz decomposition (see Problem (35)) of the displacement vector.

2.1. The FEM-BEM coupling for the standard vector formulation

In this section we consider the standard vector formulation (1), defined in the finite computational domain Ω, with the additional TD-NRBC. Then, for its numerical solution, we couple the chosen FEM with the discretization of the TD-NRBC, the latter obtained by applying a CQ-collocation BEM.

To define this latter, we introduce the following integral operators associated with the integral formulation of the elastodynamic equation:

$$\begin{aligned} \mathcal{U}_i \mathbf{t}^e(\mathbf{x},t) &= \sum_{\ell=1}^{2} \int_0^t \int_{\mathcal{B}} U^*_{i\ell}(\mathbf{x}-\mathbf{y},t-s)\mathrm{t}^e_\ell(\mathbf{y},s)\,\mathrm{d}\mathcal{B}_{\mathbf{y}}\mathrm{d}s \\ \mathcal{T}_i \mathbf{u}^e(\mathbf{x},t) &= \sum_{\ell=1}^{2} \int_0^t \int_{\mathcal{B}} T^*_{i\ell}(\mathbf{x}-\mathbf{y},t-s)\mathrm{u}^e_\ell(\mathbf{y},s)\,\mathrm{d}\mathcal{B}_{\mathbf{y}}\mathrm{d}s \end{aligned} \tag{2}$$

where $U^*_{i\ell}$ and $T^*_{i\ell}$, $i=1,2$, are the displacement and traction fundamental solutions, respectively (see [17] for their expression in the space-time domain), and t^e_ℓ is the ℓ-component of the traction vector $\mathbf{t}^e$ associated with $\mathbf{u}^e$.

The TD-NRBC associated with Problem (1), and defined on $\mathcal{B}$, has the following representation:

$$\frac{1}{2}\mathrm{u}^e_i(\mathbf{x},t) = \mathcal{U}_i \mathbf{t}^e(\mathbf{x},t) - \mathcal{T}_i \mathbf{u}^e(\mathbf{x},t) + I_{\mathrm{u}_{i,0}}(\mathbf{x},t) \; + I_{\mathrm{z}_{i,0}}(\mathbf{x},t) + I_{\mathrm{f}_i}(\mathbf{x},t), \quad i=1,2, \tag{3}$$

where the volume integrals are defined by

$$\begin{aligned} I_{\mathrm{u}_{i,0}}(\mathbf{x},t) &:= \sum_{\ell=1}^{2} \frac{\partial}{\partial t} \int_{\Omega^e} U^*_{i\ell}(\mathbf{x}-\mathbf{y},t)\mathrm{u}_{\ell,0}(\mathbf{y},t)\mathrm{d}\mathbf{y} \\ I_{\mathrm{z}_{i,0}}(\mathbf{x},t) &:= \sum_{\ell=1}^{2} \int_{\Omega^e} U^*_{i\ell}(\mathbf{x}-\mathbf{y},t)\mathrm{z}_{\ell,0}(\mathbf{y},t)\mathrm{d}\mathbf{y} \\ I_{\mathrm{f}_i}(\mathbf{x},t) &:= \sum_{\ell=1}^{2} \int_0^t \int_{\Omega^e} U^*_{i\ell}(\mathbf{x}-\mathbf{y},t-s)\mathrm{f}_\ell(\mathbf{y},s)\mathrm{d}\mathbf{y}\mathrm{d}s, \end{aligned} \tag{4}$$

with $\mathbf{f}=(\mathrm{f}_1,\mathrm{f}_2)$, $\mathbf{u}_0=(\mathrm{u}_{1,0},\mathrm{u}_{2,0})$ and $\mathbf{z}_0=(\mathrm{z}_{1,0},\mathrm{z}_{2,0})$. The details of the time dependent relation (3) associated with Problem (1) can be found, for example, in [16, 3].

From now on, to simplify the description, we assume that the local supports of $\mathbf{u}_0$, $\mathbf{z}_0$ and $\mathbf{f}$ are contained in Ω, so that $I_{\mathrm{u}_{i,0}} = I_{\mathrm{z}_{i,0}} = I_{\mathrm{f}_i} = 0$, $i=1,2$. In Example 3 of Section 3, we will show the treatment of an exterior source whose support is contained in $\mathcal{D}$.

By introducing the symmetric second order strain tensor $\boldsymbol{\varepsilon}$ defined as

$$\boldsymbol{\varepsilon}_{ij}(\mathbf{w})(\mathbf{x},t) := \frac{1}{2}\left(\frac{\partial w_i}{\partial x_j} + \frac{\partial w_j}{\partial x_i}\right)(\mathbf{x},t), \quad i,j = 1,2,$$

for $\mathbf{w}(\mathbf{x},t) = (w_1(\mathbf{x},t), w_2(\mathbf{x},t))$, and the corresponding stress tensor

$$\boldsymbol{\sigma}(\mathbf{w})(\mathbf{x},t) := 2\mu\boldsymbol{\varepsilon}(\mathbf{w})(\mathbf{x},t) + \lambda(\operatorname{div}\mathbf{w}(\mathbf{x},t))\mathbf{I},$$

where $\mathbf{I}$ denotes the 2×2 identity matrix, it is possible to rewrite the first equation of Problem (1) in the following equivalent form:

$$\rho\,\frac{\partial^2 \mathbf{u}^e}{\partial t^2}(\mathbf{x},t) - \nabla\cdot\boldsymbol{\sigma}(\mathbf{u}^e)(\mathbf{x},t) = \mathbf{f}(\mathbf{x},t), \quad (\mathbf{x},t)\in\Omega^e\times(0,T] \tag{5}$$

where, we recall, the divergence of a tensor $\boldsymbol{\sigma}$ is defined as:

$$(\nabla\cdot\boldsymbol{\sigma})_i = \sum_{j=1}^{2}\frac{\partial\sigma_{ij}}{\partial x_j}, \quad i = 1,2.$$

Combining (5) and (3), and imposing the continuity conditions of the vector field and of its traction along the artificial boundary $\mathcal{B}$, the model problem to determine the solution $\mathbf{u} := \mathbf{u}^e_\Omega$ (defined in the domain of interest Ω) reduces to:

$$\begin{cases} \rho\,\dfrac{\partial^2\mathbf{u}}{\partial t^2}(\mathbf{x},t) - \nabla\cdot\boldsymbol{\sigma}(\mathbf{u})(\mathbf{x},t) & = \mathbf{f}(\mathbf{x},t) \quad (\mathbf{x},t)\in\Omega\times(0,T] \\ \mathbf{u}(\mathbf{x},t) & = \mathbf{g}(\mathbf{x},t) \quad (\mathbf{x},t)\in\Gamma\times(0,T] \\ \frac{1}{2}\mathbf{u}(\mathbf{x},t) + \boldsymbol{\mathcal{U}}\mathbf{t}(\mathbf{x},t) + \boldsymbol{\mathcal{T}}\mathbf{u}(\mathbf{x},t) & = \mathbf{0} \quad (\mathbf{x},t)\in\mathcal{B}\times(0,T] \\ \mathbf{u}(\mathbf{x},0) & = \mathbf{u}_0(\mathbf{x}) \quad \mathbf{x}\in\Omega \\ \mathbf{u}_t(\mathbf{x},0) & = \mathbf{z}_0(\mathbf{x}) \quad \mathbf{x}\in\Omega, \end{cases} \tag{6}$$

where we have set $\mathbf{t} = \boldsymbol{\sigma}\cdot\mathbf{n} = -\boldsymbol{\sigma}\cdot\mathbf{n}_{\mathcal{D}} = -\mathbf{t}^e$, $\boldsymbol{\mathcal{U}}\mathbf{t} = (\mathcal{U}_1\mathbf{t},\mathcal{U}_2\mathbf{t})$ and $\boldsymbol{\mathcal{T}}\mathbf{u} = (\mathcal{T}_1\mathbf{u},\mathcal{T}_2\mathbf{u})$.

2.1.1. Variational formulation of the PDE in the interior domain

To describe the variational formulation of Problem (6), we use the notations $\mathbf{u}(t)(\mathbf{x}) := \mathbf{u}(\mathbf{x},t)$, $\mathbf{t}(t)(\mathbf{x}) := \mathbf{t}(\mathbf{x},t)$ and we introduce the spaces

$$\boldsymbol{V} = [H^1(\Omega)]^2, \quad \mathbf{X} = [H^{-1/2}(\mathcal{B})]^2, \quad \boldsymbol{W} = \left\{\mathbf{w}\in[H^1(\Omega)]^2 : \mathbf{w}_{|\Gamma} = \mathbf{0}\right\},$$

H^α being the classical Sobolev space of order α and $H^{-1/2}(\mathcal{B})$ the dual of $H^{1/2}(\mathcal{B})$. For simplicity, here and in the sequel we omit the use of the trace operator to indicate the restriction to a boundary of an element of $\boldsymbol{V}$.

Recalling the definition of the interior tensor product

$$\boldsymbol{\sigma}\colon\boldsymbol{\varepsilon} = \sum_{i,j=1}^{2}\sigma_{ij}\varepsilon_{ij},$$

to write the variational formulation associated with the first two equations of Problem (6), we define the bilinear form

$$a(\mathbf{v},\mathbf{w}) = \int_\Omega \boldsymbol{\sigma}(\mathbf{v})(\mathbf{x})\colon\boldsymbol{\varepsilon}(\mathbf{w})(\mathbf{x})\mathrm{d}\mathbf{x}, \qquad \mathbf{v},\mathbf{w}\in\boldsymbol{V}$$

the standard $[L^2(\Omega)]^2$ scalar product

$$(\mathbf{v},\mathbf{w})_\Omega = \int_\Omega \mathbf{v}(\mathbf{x})\cdot\mathbf{w}(\mathbf{x})\mathrm{d}\mathbf{x}, \qquad \mathbf{v},\mathbf{w}\in\boldsymbol{V}$$

and the bilinear form associated with the duality product

$$b(\boldsymbol{\lambda},\boldsymbol{\eta}) := \langle \boldsymbol{\lambda},\boldsymbol{\eta}\rangle_{\mathcal{B}}, \qquad \boldsymbol{\lambda}\in\mathbf{X},\boldsymbol{\eta}\in[H^{1/2}(\mathcal{B})]^2.$$

The variational formulation of (6) then reads: for any $t\in(0,T]$, find $\mathbf{u}(t)\in\boldsymbol{V}$ and $\mathbf{t}(t)\in\mathbf{X}$ such that

$$\rho\,\frac{d^2}{dt^2}(\mathbf{u}(t),\mathbf{w})_\Omega + a(\mathbf{u}(t),\mathbf{w}) - b(\mathbf{t}(t),\mathbf{w}) = (\mathbf{f}(t),\mathbf{w})_\Omega,$$

holds for all $\mathbf{w}\in\boldsymbol{W}$.

Finally, the model problem, where we consider the weak formulation of the interior elastodynamic equation coupled with the strong formulation of the TD-NRBC, takes the following form: for any $t\in(0,T]$, find $\mathbf{u}(t)\in\boldsymbol{V}$ and $\mathbf{t}(t)\in\mathbf{X}$ such that

$$\begin{cases} \rho\dfrac{d^2}{dt^2}(\mathbf{u}(t),\mathbf{w})_\Omega + a(\mathbf{u}(t),\mathbf{w}) - b(\mathbf{t}(t),\mathbf{w}) = (\mathbf{f}(t),\mathbf{w})_\Omega \quad \text{for all}\,\mathbf{w}\in\boldsymbol{W} \\ \dfrac{1}{2}\mathbf{u}(t)(\mathbf{x}) + \boldsymbol{\mathcal{U}}\mathbf{t}(t)(\mathbf{x}) + \boldsymbol{\mathcal{T}}\mathbf{u}(t)(\mathbf{x}) = \mathbf{0} \qquad\qquad \mathbf{x}\in\mathcal{B} \end{cases} \tag{7}$$

with initial conditions $\mathbf{u}(0)(\mathbf{x}) = \mathbf{u}_0(\mathbf{x})$, $\mathbf{u}_t(0)(\mathbf{x}) = \mathbf{z}_0(\mathbf{x})$ and the boundary condition $\mathbf{u} = \mathbf{g}$ on Γ.

In the following sections we describe the numerical procedure we adopt to approximate the TD-NRBC in (7). We consider the numerical approach which combines the time integral discretization by using a Lubich second-order time convolution quadrature (see [12]) with a continuous piecewise linear space collocation method.

2.1.2. Discretization of the TD-NRBC

Time discretization.. We consider a uniform partition of the interval $[0,T]$ into N steps of equal length $\Delta_t = T/N$ and we collocate the second equation of (7) at the time instants $t_n = n\Delta_t$, $n = 0,\dots,N$. Then we approximate the time integrals therein involved (see formula (2)) by means of the convolution quadrature formula proposed by Lubich in [12]. In particular, denoting by $\mathbf{t}^n(\mathbf{x})\approx\mathbf{t}(t_n)(\mathbf{x})$ and $\mathbf{u}^n(\mathbf{x})\approx\mathbf{u}(t_n)(\mathbf{x})$ the approximations of the traction and displacement unknowns on $\mathcal{B}$ at the discrete time instants t_n, we get: for $i=1,2$ and $n=0,\dots,N$

$$\begin{aligned} \mathcal{U}_i\mathbf{t}(\mathbf{x},t_n) &\approx \sum_{\ell=1}^{2}\sum_{j=0}^{n}\int_{\mathcal{B}} \omega_{n-j}(\Delta_t;\widehat{U}^*_{i\ell}(r))\,\mathrm{t}^j_\ell(\mathbf{y})\,\mathrm{d}\mathcal{B}_{\mathbf{y}} \\ \mathcal{T}_i\mathbf{u}(\mathbf{x},t_n) &\approx \sum_{\ell=1}^{2}\sum_{j=0}^{n}\int_{\mathcal{B}} \omega_{n-j}(\Delta_t;\widehat{T}^*_{i\ell}(r))\,\mathrm{u}^j_\ell(\mathbf{y})\,\mathrm{d}\mathcal{B}_{\mathbf{y}}, \end{aligned} \tag{8}$$

where $r = \|\mathbf{x}-\mathbf{y}\|$. In (8) the quadrature coefficients

$$\omega_j(\Delta_t;\widehat{W}) = \frac{\varrho^{-j}}{2\pi}\int_0^{2\pi}\widehat{W}\left(\frac{\gamma(\varrho\mathrm{e}^{\imath\vartheta})}{\Delta_t}\right)\mathrm{e}^{-\imath j\vartheta}\mathrm{d}\vartheta \tag{9}$$

are associated with the Laplace transform $\widehat{W}$ of the convolution kernel $W = U^*_{i\ell}, T^*_{i\ell}$. In (9) the function $\gamma(z) = 3/2 - 2z + 1/2z^2$ is the characteristic quotient of the BDF method of order 2, $\imath$ is the imaginary unit and ϱ is such that for $|z|\le\varrho$ the corresponding $\gamma(z)$ lies in the domain of analyticity of $\widehat{W}$. The integrals in (9) are efficiently computed by using the trapezoidal rule

$$\omega_j(\Delta_t;\widehat{W}) \approx \frac{\varrho^{-j}}{L}\sum_{l=0}^{L-1}\widehat{W}\left(\frac{\gamma(\varrho\mathrm{e}^{\imath l\frac{2\pi}{L}})}{\Delta_t}\right)\mathrm{e}^{-\imath jl\frac{2\pi}{L}}, \qquad j=0,\dots,N \tag{10}$$

based on the uniform partitioning of $[0, 2\pi]$ in L subintervals. The quadrature coefficients $\omega_j(\Delta_t; \widehat{W})$ are then computed simultaneously using the FFT, with $O(N \log N)$ flops. Assuming that W is computed with a relative accuracy bounded by ε, Lubich has shown (see [13]) that the choice $L = 2N$ and $\varrho^N = \sqrt{\varepsilon}$ leads to an approximation of ω_j with relative error of size $\sqrt{\varepsilon}$.

For completeness, we report here the expressions of the Laplace transforms $\widehat{W}$, involved in (9), which can be found in [3]:

$$\widehat{U}^*_{i\ell}(r,s) = \frac{1}{2\pi\rho v_S^2}\Big(\psi(r,s)\delta_{i\ell} - \chi(r,s) r_{,i} r_{,\ell}\Big) \tag{11}$$

$$\begin{aligned}\widehat{T}^*_{i\ell}(r,s) =& \frac{1}{2\pi}\left\{\left[\frac{\partial\psi}{\partial r}(r,s) - \frac{\chi(r,s)}{r}\right]\left(\delta_{i\ell}\frac{\partial r}{\partial \mathbf{n}_\mathcal{D}} + r_{,\ell} n_i\right) - 2\frac{\chi(r,s)}{r}\left(r_{,i} n_\ell - 2 r_{,i} r_{,\ell}\frac{\partial r}{\partial \mathbf{n}_\mathcal{D}}\right)\right. \\ & \left. -2\frac{\partial\chi}{\partial r}(r,s) r_{,i} r_{,\ell}\frac{\partial r}{\partial \mathbf{n}_\mathcal{D}} + \left(\frac{v_P^2}{v_S^2} - 2\right)\left[\frac{\partial\psi}{\partial r}(r,s) - \frac{\partial\chi}{\partial r}(r,s) - \frac{\chi(r,s)}{r}\right] r_{,i} n_\ell\right\},\end{aligned} \tag{12}$$

where $r_{,i} := \partial_{y_i} r$, $\delta_{i\ell}$ is the Kronecker delta and v_P, v_S denote the so-called P- and S-wave speeds, defined by the Lamé constants through the relationships:

$$v_P = \sqrt{\frac{\lambda + 2\mu}{\rho}}, \qquad v_S = \sqrt{\frac{\mu}{\rho}}. \tag{13}$$

The functions ψ and χ in (11) and (12) are defined as follows:

$$\psi(r,s) = K_0\left(\frac{rs}{v_S}\right) + \left(\frac{v_S}{rs}\right)\left[K_1\left(\frac{rs}{v_S}\right) - \frac{v_S}{v_P} K_1\left(\frac{rs}{v_P}\right)\right], \tag{14}$$

$$\chi(r,s) = K_2\left(\frac{rs}{v_S}\right) - \left(\frac{v_S}{v_P}\right)^2 K_2\left(\frac{rs}{v_P}\right), \tag{15}$$

where K_i, $i = 0, 1, 2$, is the second-kind modified Bessel functions of order i.

From these, using the relations $K_0'(z) = -K_1(z)$, $K_1'(z) = -K_0(z) - 1/z K_1(z)$ and $K_2'(z) = -2/z K_2(z) - K_1(z)$, we easily obtain (see [10])

$$\frac{\partial\psi}{\partial r}(r,s) = -\frac{1}{r}\left[\chi(r,s) + \frac{rs}{v_S} K_1\left(\frac{rs}{v_S}\right)\right] \tag{16}$$

and

$$\frac{\partial\chi}{\partial r}(r,s) = -\frac{1}{r}\left[\frac{rs}{v_S} K_1\left(\frac{rs}{v_S}\right) - \left(\frac{v_S}{v_P}\right)^2 \frac{rs}{v_P} K_1\left(\frac{rs}{v_P}\right) + 2\chi(r,s)\right]. \tag{17}$$

For further details see [8].

Space discretization. To describe the space discretization, we assume that the boundary $\mathcal{B}$ is represented by a smooth global parametric representation defined on the unit interval:

$$\mathbf{x} = \boldsymbol{\eta}(\vartheta) = (\eta_1(\vartheta), \eta_2(\vartheta)), \qquad \vartheta \in [0,1]. \tag{18}$$

Using this representation, we first reduce the integral on $\mathcal{B}$ to the equivalent one defined on the parametrization interval $[0, 1]$. Then, after having taken the uniform partition of $[0, 1]$ into M subintervals identified by the equidistant nodes $\{\vartheta_k\}_{k=1}^{M+1}$, we define the associated continuous piecewise linear function, whose basis functions are denoted by $\{N_k\}_{k=1}^{M+1}$.

The unknown functions $\mathrm{t}_\ell^n(\mathbf{x})$ and $\mathrm{u}_\ell^n(\mathbf{x})$, $\ell = 1, 2$, $\mathbf{x} \in \mathcal{B}$ are approximated as follows:

$$\mathrm{t}_\ell^n(\boldsymbol{\eta}(\vartheta)) \approx \sum_{k=1}^{M+1} \mathrm{t}_\ell^{k,n} N_k(\vartheta), \quad \mathrm{u}_\ell^n(\boldsymbol{\eta}(\vartheta)) \approx \sum_{k=1}^{M+1} \mathrm{u}_\ell^{k,n} N_k(\vartheta) \tag{19}$$

where the coefficients $\mathrm{t}_\ell^{k,n}$ and $\mathrm{u}_\ell^{k,n}$ represents the unknown nodal values at $\mathbf{x}_k = \boldsymbol{\eta}(\vartheta_k)$. Taking into account that the curve $\mathcal{B}$ is closed, we set $\mathrm{t}_\ell^{1,j} = \mathrm{t}_\ell^{M+1,j}$ and $\mathrm{u}_\ell^{1,j} = \mathrm{u}_\ell^{M+1,j}$. Finally, by collocating the fully discretized equation at the points ϑ_m, $m = 1, \ldots, M$, we end up with the following full approximation of the TD-NRBC:

$$\sum_{\ell=1}^{2} \left(\frac{1}{2}\delta_{i\ell}\mathbb{I} + \mathbb{T}_{i\ell}^0 \right) \mathbf{u}_\ell^{\mathcal{B},n} + \sum_{\ell=1}^{2} \sum_{j=0}^{n-1} \mathbb{T}_{i\ell}^{n-j} \mathbf{u}_\ell^{\mathcal{B},j} + \sum_{\ell=1}^{2} \mathbb{U}_{i\ell}^0 \mathbf{t}_\ell^{\mathcal{B},n} + \sum_{\ell=1}^{2} \sum_{j=0}^{n-1} \mathbb{U}_{i\ell}^{n-j} \mathbf{t}_\ell^{\mathcal{B},j} = 0, \quad i = 1, 2 \tag{20}$$

in the unknown vectors $\mathbf{t}_\ell^{\mathcal{B},n} = (\mathrm{t}_\ell^{1,n}, \ldots, \mathrm{t}_\ell^{M,n})^T$ and $\mathbf{u}_\ell^{\mathcal{B},n} = (\mathrm{u}_\ell^{1,n}, \ldots, \mathrm{u}_\ell^{M,n})^T$, with $\ell = 1, 2$ and $n = 0, \ldots, N$. The symbol $\mathbb{I}$ denotes the identity matrix of order M, while the matrix entries of $\mathbb{U}^n$ and $\mathbb{T}^n$ are given by (see [8] for details on their computation)

$$(\mathbb{U}_{i\ell}^n)_{m,k} = \frac{1}{2\pi} \frac{\varrho^{-n}}{L} \sum_{l=0}^{L-1} \left(\int_0^1 \widehat{U}_{i\ell}^* \left(r_m(\vartheta), z_l \right) N_k(\vartheta) \, \|\boldsymbol{\eta}'(\vartheta)\| \, \mathrm{d}\vartheta \right) \mathrm{e}^{-\frac{\imath n l 2\pi}{L}} \tag{21}$$

and

$$(\mathbb{T}_{i\ell}^n)_{m,k} = \frac{1}{2\pi} \frac{\varrho^{-n}}{L} \sum_{l=0}^{L-1} \left(\int_0^1 \widehat{T}_{i\ell}^* \left(r_m(\vartheta), z_l \right) N_k(\vartheta) \, \|\boldsymbol{\eta}'(\vartheta)\| \, \mathrm{d}\vartheta \right) \mathrm{e}^{-\frac{\imath n l 2\pi}{L}}, \tag{22}$$

where $z_l := \gamma(\varrho \mathrm{e}^{il2\pi/L})/\Delta_t$ and $r_m(\vartheta) = \|\boldsymbol{\eta}(\vartheta_m) - \boldsymbol{\eta}(\vartheta)\|$.

From the computational point of view, supposing to know $\mathbf{u}_\ell^{\mathcal{B},j}$ and $\mathbf{t}_\ell^{\mathcal{B},j}$ at the time instants t_j, $j = 0, \cdots, n-1$, the NRBC at t_n is given by

$$\sum_{\ell=1}^{2} \left(\frac{1}{2}\delta_{i\ell}\mathbb{I} + \mathbb{T}_{i\ell}^0 \right) \mathbf{u}_\ell^{\mathcal{B},n} + \sum_{\ell=1}^{2} \mathbb{U}_{i\ell}^0 \mathbf{t}_\ell^{\mathcal{B},n} = - \sum_{\ell=1}^{2} \sum_{j=0}^{n-1} \mathbb{T}_{i\ell}^{n-j} \mathbf{u}_\ell^{\mathcal{B},j} - \sum_{\ell=1}^{2} \sum_{j=0}^{n-1} \mathbb{U}_{i\ell}^{n-j} \mathbf{t}_\ell^{\mathcal{B},j}, \quad i = 1, 2. \tag{23}$$

2.1.3. Discretization of the interior vector PDE equation

Time discretization. To derive the complete numerical method we propose to solve (7), we first describe the time discretization of its first equation. We perform this latter by using the Crank-Nicolson scheme, of second order and well suited even for long time integration intervals. Of course, other methods could be considered as well, in particular those of explicit type.

Thus, we introduce the new unknown vector function $\mathbf{z} := \frac{\partial \mathbf{u}}{\partial t}$ and we rewrite (7) as follows:

$$\begin{cases} \rho \frac{d}{dt}(\mathbf{z}(t), \mathbf{w})_\Omega + a(\mathbf{u}(t), \mathbf{w}) - b(\mathbf{t}(t), \mathbf{w}) & = (\mathbf{f}(t), \mathbf{w})_\Omega \quad \text{for all } \mathbf{w} \in \boldsymbol{W},\ t \in (0, T] \\ \frac{\partial \mathbf{u}}{\partial t}(\mathbf{x}, t) & = \mathbf{z}(\mathbf{x}, t) \quad \mathbf{x} \in \Omega,\ t \in (0, T] \\ \frac{1}{2}\mathbf{u}(\mathbf{x}, t) + \boldsymbol{\mathcal{U}}\mathbf{t}(\mathbf{x}, t) + \boldsymbol{\mathcal{T}}\mathbf{u}(\mathbf{x}, t) & = \mathbf{0} \quad \mathbf{x} \in \mathcal{B},\ t \in (0, T] \\ \mathbf{u}(\mathbf{x}, 0) & = \mathbf{u}_0(\mathbf{x}) \quad \mathbf{x} \in \Omega \\ \mathbf{z}(\mathbf{x}, 0) & = \mathbf{z}_0(\mathbf{x}) \quad \mathbf{x} \in \Omega. \end{cases} \tag{24}$$

Denoting by $\mathbf{u}^n(\mathbf{x}) \approx \mathbf{u}(\mathbf{x}, t_n)$, $\mathbf{z}^n(\mathbf{x}) \approx \mathbf{z}(\mathbf{x}, t_n)$, $\mathbf{t}^n(\mathbf{x}) \approx \mathbf{t}(\mathbf{x}, t_n)$ and $\mathbf{f}^n(\mathbf{x}) \approx \mathbf{f}(\mathbf{x}, t_n)$ the approximations of $\mathbf{u}$, $\mathbf{z}$, $\mathbf{t}$ and $\mathbf{f}$ at the time instant t_n, and applying the Crank-Nicolson discretization to the first two equations in (24), we get

$$\begin{cases} \rho \left(\dfrac{\mathbf{z}^{n+1} - \mathbf{z}^n}{\Delta_t}, \mathbf{w} \right)_\Omega + a\left(\dfrac{\mathbf{u}^{n+1} + \mathbf{u}^n}{2}, \mathbf{w} \right) - b\left(\dfrac{\mathbf{t}^{n+1} + \mathbf{t}^n}{2}, \mathbf{w} \right) = \left(\dfrac{\mathbf{f}^{n+1} + \mathbf{f}^n}{2}, \mathbf{w} \right)_\Omega, \\ \dfrac{\mathbf{u}^{n+1} - \mathbf{u}^n}{\Delta_t} = \dfrac{\mathbf{z}^{n+1} + \mathbf{z}^n}{2}. \end{cases}$$

From the second relation we obtain:

$$\mathbf{z}^{n+1} = \frac{2}{\Delta_t}(\mathbf{u}^{n+1} - \mathbf{u}^n) - \mathbf{z}^n \tag{25}$$

which, inserted in the first relation, leads to

$$\begin{aligned}\rho\,(\mathbf{u}^{n+1},\mathbf{w})_\Omega+\frac{\Delta_t^2}{4}a(\mathbf{u}^{n+1},\mathbf{w})-\frac{\Delta_t^2}{4}b(\mathbf{t}^{n+1},\mathbf{w}) &= \rho\,(\mathbf{u}^{n},\mathbf{w})_\Omega-\frac{\Delta_t^2}{4}a(\mathbf{u}^{n},\mathbf{w})+\frac{\Delta_t^2}{4}b(\mathbf{t}^{n},\mathbf{w})\\ &+ \rho\Delta_t\,(\mathbf{z}^n,\mathbf{w})_\Omega+\frac{\Delta_t^2}{4}(\mathbf{f}^{n+1}+\mathbf{f}^n,\mathbf{w})_\Omega. \quad (26)\end{aligned}$$

Space discretization by finite elements. For the space finite element discretization, we define a regular decomposition $\mathcal{T}_h=\{K\}$ of Ω into triangles and we denote by h its mesh size. This defines a polygonal domain Ω_Δ, having inner and outer boundaries Γ_Δ and $\mathcal{B}_\Delta$, respectively. Then, we replace Ω by Ω_Δ and $\mathcal{B}$ by $\mathcal{B}_\Delta$ in (26). We remark that, for the space discretization of the TD-NRBC we have used the parametric representation of $\mathcal{B}$, instead of that of $\mathcal{B}_\Delta$. Note however that, in spite of this boundary discrepancy, the final discrete system will involve only the unknown values at the common boundary mesh points, $\mathcal{B}_\Delta$ being nothing but a piecewise linear interpolant of $\mathcal{B}$.

Denoting by $f_{|_D}$ the restriction of a function f on a domain D, let

$$\boldsymbol{V}_h=\{\mathbf{v}_h\in[C^0(\Omega)]^2:\mathbf{v}_{h_{|K}}\in[\mathbb{P}^1(K)]^2,K\in\mathcal{T}_h,\},$$

$$\boldsymbol{W}_h=\{\mathbf{w}_h\in[C^0(\Omega)]^2:\mathbf{w}_{h_{|K}}\in[\mathbb{P}^1(K)]^2,K\in\mathcal{T}_h,\mathbf{w}_{h_{|\Gamma_\Delta}}=0\}$$

be the spaces of piecewise linear vector polynomials of degree 1 associated with the mesh $\mathcal{T}_h$.

Let $\mathcal{S}$ be the set of the indices of the nodes $\{\mathbf{x}_i\}_{i\in\mathcal{S}}$ of the triangular mesh, not including those lying on Γ, and $\{N_i^\Omega\}_{i\in\mathcal{S}}$ the standard piecewise linear finite element basis functions. Denoting by $S=\#\mathcal{S}$ the total number of nodes, a natural choice for the set of the basis functions of $\boldsymbol{V}_h$ is given by the $2S$ columns of the matrix

$$\mathbf{N}^\Omega(\mathbf{x}):=\begin{bmatrix} N_1^\Omega(\mathbf{x}) & N_2^\Omega(\mathbf{x}) & \cdots & N_S^\Omega(\mathbf{x}) & 0 & 0 & \cdots & 0\\ 0 & 0 & \cdots & 0 & N_1^\Omega(\mathbf{x}) & N_2^\Omega(\mathbf{x}) & \cdots & N_S^\Omega(\mathbf{x})\end{bmatrix}.$$

Then, for the unknown vector function $\mathbf{u}^n(\mathbf{x})=(\mathrm{u}_1^n(\mathbf{x}),\mathrm{u}_2^n(\mathbf{x}))^T$, we consider its finite element approximation defined as follows:

$$\mathbf{u}_h^n(\mathbf{x})=\begin{bmatrix}\mathrm{u}_{1,h}^n(\mathbf{x})\\ \mathrm{u}_{2,h}^n(\mathbf{x})\end{bmatrix}=\mathbf{N}^\Omega(\mathbf{x})\mathbf{u}^n=\begin{bmatrix}\sum_{i=1}^S \mathrm{u}_1^{i,n}N_i^\Omega(\mathbf{x})\\ \sum_{i=1}^S \mathrm{u}_2^{i,n}N_i^\Omega(\mathbf{x})\end{bmatrix},\quad\text{with}\quad \mathbf{u}^n=\begin{bmatrix}\mathbf{u}_1^n\\ \mathbf{u}_2^n\end{bmatrix}$$

and where

$$\mathbf{u}_1^n=\left[\mathrm{u}_1^{1,n},\mathrm{u}_1^{2,n},\cdots,\mathrm{u}_1^{S,n}\right]^T\quad\text{and}\quad\mathbf{u}_2^n=\left[\mathrm{u}_2^{1,n},\mathrm{u}_2^{2,n},\cdots,\mathrm{u}_2^{S,n}\right]^T$$

are the unknown nodal values associated with the nodes of the triangular mesh.

Moreover, let $\mathbf{X}_h\subset\mathbf{X}$ be the space of piecewise linear continuous vector functions defined on the boundary $\mathcal{B}$ by the non-vanishing finite element basis functions $\mathbf{N}^\mathcal{B}(\mathbf{x})=\mathbf{N}^\Omega_{|_\mathcal{B}}(\mathbf{x})$. Thus, proceeding analogously as before, and recalling that M denotes the number of mesh points that belong to the boundary $\mathcal{B}$, we introduce the following $2M$ columns matrix for the basis $\mathbf{N}^\mathcal{B}(\mathbf{x})$:

$$\mathbf{N}^\mathcal{B}(\mathbf{x})=\begin{bmatrix} N_1^\mathcal{B}(\mathbf{x}) & N_2^\mathcal{B}(\mathbf{x}) & \cdots & N_M^\mathcal{B}(\mathbf{x}) & 0 & 0 & \cdots & 0\\ 0 & 0 & \cdots & 0 & N_1^\mathcal{B}(\mathbf{x}) & N_2^\mathcal{B}(\mathbf{x}) & \cdots & N_M^\mathcal{B}(\mathbf{x})\end{bmatrix}.$$

Then, for the unknown function $\mathbf{t}^n(\mathbf{x})=(\mathrm{t}_1^n(\mathbf{x}),\mathrm{t}_2^n(\mathbf{x}))^T$, with $\mathbf{x}\in\mathcal{B}$, we introduce its finite

element approximation defined as follows:

$$\mathbf{t}_h^n(\mathbf{x}) = \begin{bmatrix} \mathrm{t}_{1,h}^n(\mathbf{x}) \\ \mathrm{t}_{2,h}^n(\mathbf{x}) \end{bmatrix} = \mathbf{N}^{\mathcal{B}}(\mathbf{x})\mathbf{t}^n = \begin{bmatrix} \sum_{i=1}^{M} \mathrm{t}_{1,i}^n N_i^{\mathcal{B}}(\mathbf{x}) \\ \sum_{i=1}^{M} \mathrm{t}_{2,i}^n N_i^{\mathcal{B}}(\mathbf{x}) \end{bmatrix}, \quad \text{with} \quad \mathbf{t}^n = \begin{bmatrix} \mathbf{t}_1^n \\ \mathbf{t}_2^n \end{bmatrix}$$

and where

$$\mathbf{t}_1^n = \left[\mathrm{t}_1^{1,n}, \mathrm{t}_1^{2,n}, \cdots, \mathrm{t}_1^{M,n}\right]^T \quad \text{and} \quad \mathbf{t}_2^n = \left[\mathrm{t}_2^{1,n}, \mathrm{t}_2^{2,n}, \cdots, \mathrm{t}_2^{M,n}\right]^T$$

are the vectors of the unknown nodal values.

The Galerkin formulation of (26) then reads as follows: for each $n = 0, \cdots, N-1$, find $(\mathbf{u}_h^{n+1}, \mathbf{t}_h^{n+1}) \in \boldsymbol{V}_h \times \mathbf{X}_h$ such that, for all $\mathbf{w}_h \in \boldsymbol{W}_h$

$$\begin{aligned} \rho(\mathbf{u}_h^{n+1}, \mathbf{w}_h)_\Omega + \frac{\Delta_t^2}{4} a(\mathbf{u}_h^{n+1}, \mathbf{w}_h) - \frac{\Delta_t^2}{4} b(\mathbf{t}_h^{n+1}, \mathbf{w}_h) = \rho(\mathbf{u}_h^n, \mathbf{w}_h)_\Omega - \frac{\Delta_t^2}{4} a(\mathbf{u}_h^n, \mathbf{w}_h) \\ + \frac{\Delta_t^2}{4} b(\mathbf{t}_h^n, \mathbf{w}_h) + \Delta_t \rho(\mathbf{z}_h^n, \mathbf{w}_h)_\Omega + \frac{\Delta_t^2}{4}(\mathbf{f}^{n+1} + \mathbf{f}^n, \mathbf{w}_h)_\Omega. \end{aligned} \tag{27}$$

To write the discrete variational formulation (27) in matrix form, we split the total set of indices $\mathcal{S} = \mathcal{S}^I \cup \mathcal{S}^{\mathcal{B}}$, into the set $\mathcal{S}^I$ of interior mesh nodes and $\mathcal{S}^{\mathcal{B}}$ of the mesh nodes lying on the artificial boundary $\mathcal{B}$. Then, by properly reordering the unknown coefficients of $\mathbf{u}_h^n$, we rewrite the unknown vectors $\mathbf{u}_i^n = [\mathbf{u}_i^{I,n}, \mathbf{u}_i^{\mathcal{B},n}]^T$, $i = 1, 2$, whose two components $\mathbf{u}_i^{I,n}$ and $\mathbf{u}_i^{\mathcal{B},n}$ represent the unknown values associated with the internal nodes and with those on the boundary $\mathcal{B}$, respectively. The same splitting is performed for the vector $\mathbf{z}^n$, containing the unknown coefficients of $\mathbf{z}_h^n$.

Therefore, setting $\alpha = \frac{\Delta_t^2}{4}$, the matrix form of (27) is given by

$$\Big(\mathbf{M} + \alpha\mathbf{A}\Big)\mathbf{u}^{n+1} - \alpha\mathbf{Q}\mathbf{t}^{n+1} = \Big(\mathbf{M} - \alpha\mathbf{A}\Big)\mathbf{u}^n + \alpha\mathbf{Q}\mathbf{t}^n + \Delta_t\mathbf{M}\mathbf{v}^n + \alpha\mathbf{F}^n \tag{28}$$

where, denoting by $\mathbf{N}_i^\Omega$ and $\mathbf{N}_i^{\mathcal{B}}$ the i-th column of the matrix $\mathbf{N}^\Omega$ and $\mathbf{N}^{\mathcal{B}}$ respectively, the elements of the mass and stiffness matrices are

$$\mathbf{M}_{ij} = \rho\left(\mathbf{N}_i^\Omega, \mathbf{N}_j^\Omega\right)_\Omega, \quad \mathbf{A}_{ij} = a(\mathbf{N}_i^\Omega, \mathbf{N}_j^\Omega), \quad i, j = 1, \cdots, 2S \tag{29}$$

while those of $\mathbf{Q}$ are given by

$$\mathbf{Q}_{ij} = \int_{\mathcal{B}} \mathbf{N}_i^\Omega \cdot \mathbf{N}_j^{\mathcal{B}}, \quad i = 1, \cdots, 2S,\ j = 1, \cdots, 2M. \tag{30}$$

The term $\mathbf{F}^n$ in (28) is the column vector whose components are defined by

$$\mathbf{F}_j^n = (\mathbf{f}^{n+1} + \mathbf{f}^n, \mathbf{N}_j^\Omega)_\Omega, \qquad j = 1, \cdots, 2S.$$

To write the matrix form of the final linear system, it is useful to introduce the following blocks

of the above matrices, based on a proper assembly of the total set of the basis functions:

$$\mathbb{M}_{11} = [\mathbf{M}_{rs}]_{r=1,\cdots,S,\ s=1,\cdots,S}, \qquad \mathbb{M}_{22} = [\mathbf{M}_{rs}]_{r=S+1,\cdots,2S,\ s=S+1,\cdots,2S};$$

$$\mathbb{M}_{12} = [\mathbf{M}_{rs}]_{r=1,\cdots,S,\ s=S+1,\cdots,2S}, \quad \mathbb{M}_{21} = [\mathbf{M}_{rs}]_{r=S+1,\cdots,2S,\ s=1,\cdots,S};$$

$$\mathbb{A}_{11} = [\mathbf{A}_{rs}]_{r=1,\cdots,S,\ s=1,\cdots,S}, \qquad \mathbb{A}_{22} = [\mathbf{A}_{rs}]_{r=S+1,\cdots,2S,\ s=S+1,\cdots,2S};$$

$$\mathbb{A}_{12} = [\mathbf{A}_{rs}]_{r=1,\cdots,S,\ s=S+1,\cdots,2S}, \qquad \mathbb{A}_{21} = [\mathbf{A}_{sr}]_{r=1,\cdots,S,s=S+1,\cdots,2S};$$

$$\mathbb{Q}_{11} = [\mathbf{Q}_{rs}]_{r=1,\cdots,S,\ s=1,\cdots,M}, \qquad \mathbb{Q}_{22} = [\mathbf{Q}_{rs}]_{r=S+1,\cdots,2S,\ s=M+1,\cdots,2M};$$

$$\mathbb{Q}_{12} = [\mathbf{Q}_{rs}]_{r=1,\cdots,S,\ s=M+1,\cdots,2M}, \quad \mathbb{Q}_{21} = [\mathbf{Q}_{rs}]_{r=S+1,\cdots,2S,\ s=1,\cdots,M};$$

$$\mathbb{F}_1^n = [\mathbf{F}_r^n]_{r=1,\cdots,S}, \qquad \mathbb{F}_2^n = [\mathbf{F}_r^n]_{r=S+1,\cdots,2S}.$$

Finally, by taking into account the splitting of the index set $\mathcal{S} = \mathcal{S}^I \cup \mathcal{S}^{\mathcal{B}}$, we further partition each of the above matrices into sub-blocks, as follows:

$$\mathbb{M}_{pq} = \begin{bmatrix} \mathbb{M}_{pq}^{II} & \mathbb{M}_{pq}^{I\mathcal{B}} \\ \mathbb{M}_{pq}^{\mathcal{B}I} & \mathbb{M}_{pq}^{\mathcal{B}\mathcal{B}} \end{bmatrix}, \qquad \mathbb{A}_{pq} = \begin{bmatrix} \mathbb{A}_{pq}^{II} & \mathbb{A}_{pq}^{I\mathcal{B}} \\ \mathbb{A}_{pq}^{\mathcal{B}I} & \mathbb{A}_{pq}^{\mathcal{B}\mathcal{B}} \end{bmatrix}, \qquad \mathbb{Q}_{pq} = \begin{bmatrix} \mathbb{Q}_{pq}^{I\mathcal{B}} \\ \mathbb{Q}_{pq}^{\mathcal{B}\mathcal{B}} \end{bmatrix}, \quad p, q = 1, 2.$$

It is worth noting that, according to the structure of the bases $\mathbf{N}^{\Omega}$ and $\mathbf{N}^{\mathcal{B}}$, we have $\mathbb{M}_{12} = \mathbb{M}_{21} = \mathbb{O}$, $\mathbb{Q}_{12} = \mathbb{Q}_{21} = \mathbb{O}$ and $\mathbb{Q}_{11}^{I\mathcal{B}} = \mathbb{Q}_{22}^{I\mathcal{B}} = \mathbb{O}$. Moreover, the following equalities hold: $\mathbb{M}_{11} = \mathbb{M}_{22}$, $\mathbb{A}_{12} = \mathbb{A}_{21}$ and $\mathbb{Q}_{11}^{\mathcal{B}\mathcal{B}} = \mathbb{Q}_{22}^{\mathcal{B}\mathcal{B}}$.

Finally, combining (28) with (23), and in accordance with the splitting of the set of the degrees of freedom, we get the following block partitioned linear system (with obvious meaning of the

notation):

$$\begin{bmatrix} \mathbb{M}_{11}^{II}+\alpha\mathbb{A}_{11}^{II} & \mathbb{M}_{11}^{I\mathcal{B}}+\alpha\mathbb{A}_{11}^{I\mathcal{B}} & \alpha\mathbb{A}_{12}^{II} & \alpha\mathbb{A}_{12}^{I\mathcal{B}} & \mathbb{O} & \mathbb{O} \\ \mathbb{M}_{11}^{\mathcal{B}I}+\alpha\mathbb{A}_{11}^{\mathcal{B}I} & \mathbb{M}_{11}^{\mathcal{B}\mathcal{B}}+\alpha\mathbb{A}_{11}^{\mathcal{B}\mathcal{B}} & \alpha\mathbb{A}_{12}^{\mathcal{B}I} & \alpha\mathbb{A}_{12}^{\mathcal{B}\mathcal{B}} & -\alpha\mathbb{Q}_{11}^{\mathcal{B}\mathcal{B}} & \mathbb{O} \\ \alpha\mathbb{A}_{21}^{II} & \alpha\mathbb{A}_{21}^{I\mathcal{B}} & \mathbb{M}_{22}^{II}+\alpha\mathbb{A}_{22}^{II} & \mathbb{M}_{22}^{I\mathcal{B}}+\alpha\mathbb{A}_{22}^{I\mathcal{B}} & \mathbb{O} & \mathbb{O} \\ \alpha\mathbb{A}_{21}^{\mathcal{B}I} & \alpha\mathbb{A}_{21}^{\mathcal{B}\mathcal{B}} & \mathbb{M}_{22}^{\mathcal{B}I}+\alpha\mathbb{A}_{22}^{\mathcal{B}I} & \mathbb{M}_{22}^{\mathcal{B}\mathcal{B}}+\alpha\mathbb{A}_{22}^{\mathcal{B}\mathcal{B}} & \mathbb{O} & -\alpha\mathbb{Q}_{22}^{\mathcal{B}\mathcal{B}} \\ \mathbb{O} & \frac{1}{2}\mathbb{I}+\mathbb{T}_{11}^{0} & \mathbb{O} & \mathbb{T}_{12}^{0} & \mathbb{U}_{11}^{0} & \mathbb{U}_{12}^{0} \\ \mathbb{O} & \mathbb{T}_{21}^{0} & \mathbb{O} & \frac{1}{2}\mathbb{I}+\mathbb{T}_{22}^{0} & \mathbb{U}_{21}^{0} & \mathbb{U}_{22}^{0} \end{bmatrix} \begin{bmatrix} \mathbf{u}_1^{I,n+1} \\ \mathbf{u}_1^{\mathcal{B},n+1} \\ \mathbf{u}_2^{I,n+1} \\ \mathbf{u}_2^{\mathcal{B},n+1} \\ \mathbf{t}_1^{\mathcal{B},n+1} \\ \mathbf{t}_2^{\mathcal{B},n+1} \end{bmatrix}$$

$$= \begin{bmatrix} \displaystyle\sum_{i=1}^{2}\sum_{*=I}^{\mathcal{B}} \left(\mathbb{M}_{1i}^{I*}-\alpha\mathbb{A}_{1i}^{I*}\right)\mathbf{u}_i^{*,n}+\Delta_t\sum_{*=I}^{\mathcal{B}}\mathbb{M}_{11}^{I*}\mathbf{z}_1^{*,n}+\alpha\mathbb{F}_1^{n,I} \\ \displaystyle\sum_{i=1}^{2}\sum_{*=I}^{\mathcal{B}} \left(\mathbb{M}_{1i}^{\mathcal{B}*}-\alpha\mathbb{A}_{1i}^{\mathcal{B}*}\right)\mathbf{u}_i^{*,n}+\alpha\mathbb{Q}_{11}^{\mathcal{B}\mathcal{B}}\mathbf{t}_1^{\mathcal{B}}+\Delta_t\sum_{*=I}^{\mathcal{B}}\mathbb{M}_{11}^{\mathcal{B}*}\mathbf{z}_1^{*,n}+\alpha\mathbb{F}_1^{n,\mathcal{B}} \\ \displaystyle\sum_{i=1}^{2}\sum_{*=I}^{\mathcal{B}} \left(\mathbb{M}_{2i}^{I*}-\alpha\mathbb{A}_{2i}^{I*}\right)\mathbf{u}_2^{*,n}+\Delta_t\sum_{*=I}^{\mathcal{B}}\mathbb{M}_{22}^{I*}\mathbf{z}_2^{*,n}+\alpha\mathbb{F}_2^{n,I} \\ \displaystyle\sum_{i=1}^{2}\sum_{*=I}^{\mathcal{B}} \left(\mathbb{M}_{2i}^{\mathcal{B}*}-\alpha\mathbb{A}_{2i}^{\mathcal{B}*}\right)\mathbf{u}_i^{*,n}+\alpha\mathbb{Q}_{22}^{\mathcal{B}\mathcal{B}}\mathbf{t}_2^{\mathcal{B}}+\Delta_t\sum_{*=I}^{\mathcal{B}}\mathbb{M}_{22}^{\mathcal{B}*}\mathbf{z}_2^{*,n}+\alpha\mathbb{F}_2^{n,\mathcal{B}} \\ \displaystyle-\sum_{i=1}^{2}\sum_{j=0}^{n-1}\mathbb{T}_{1i}^{n-j}\mathbf{u}_i^{\mathcal{B},j}-\sum_{i=1}^{2}\sum_{j=0}^{n-1}\mathbb{U}_{1i}^{n-j}\mathbf{t}_i^{\mathcal{B},j} \\ \displaystyle-\sum_{i=1}^{2}\sum_{j=0}^{n-1}\mathbb{T}_{2i}^{n-j}\mathbf{u}_i^{\mathcal{B},j}-\sum_{i=1}^{2}\sum_{j=0}^{n-1}\mathbb{U}_{2i}^{n-j}\mathbf{t}_i^{\mathcal{B},j} \end{bmatrix},$$

to which equation (25) must be added.

2.2. The FEM-BEM coupling for the new scalar approach

It is well-known (see [5]) that, using the Helmholtz decomposition of a vector field, we can decompose the unknown displacement in (1) by two unknown scalar potentials $\mathbf{u}^e = \nabla\varphi_P^e + \mathbf{curl}\,\varphi_S^e$ where, for a generic $w = w(x_1, x_2)$, $\mathbf{curl}\,w = (\partial_{x_2}w, -\partial_{x_1}w)$. The unknowns φ_P^e and φ_S^e are called Primary (or longitudinal) and Secondary (or transverse) waves.

Referring to [8] for details, we recall the main relations that allows us to rewrite Problem (1) in terms of a couple of wave equations. In particular, by using the decomposition of the Dirichlet datum on Γ

$$\nabla\varphi_P^e + \mathbf{curl}\,\varphi_S^e = \mathbf{g} \tag{31}$$

and introducing the anti-clockwise oriented unit tangent vector $\boldsymbol{\tau}_\Gamma = (n_{\Gamma,2}, -n_{\Gamma,1})$, $\mathbf{n}_\Gamma = (n_{\Gamma,1}, n_{\Gamma,2})$ being the ingoing unit normal vector on Γ, the following relations hold:

$$\frac{\partial\varphi_P^e}{\partial\mathbf{n}_\Gamma} - \frac{\partial\varphi_S^e}{\partial\boldsymbol{\tau}_\Gamma} = \mathbf{g}\cdot\mathbf{n}_\Gamma, \qquad \frac{\partial\varphi_S^e}{\partial\mathbf{n}_\Gamma} + \frac{\partial\varphi_P^e}{\partial\boldsymbol{\tau}_\Gamma} = \mathbf{g}\cdot\boldsymbol{\tau}_\Gamma. \tag{32}$$

Furthermore, after setting

$$\begin{array}{rclrcl} \varphi^e_{P,0}(\mathbf{x}) & := & \varphi^e_P(\mathbf{x},0), & \varphi^e_{S,0}(\mathbf{x}) & := & \varphi^e_S(\mathbf{x},0) \\ \bar{\varphi}^e_{P,0}(\mathbf{x}) & := & \partial_t\varphi^e_P(\mathbf{x},0), & \bar{\varphi}^e_{S,0}(\mathbf{x}) & := & \partial_t\varphi^e_S(\mathbf{x},0) \end{array} \tag{33}$$

and decomposing the initial data $\mathbf{u}_0$, $\mathbf{z}_0$, the Dirichlet datum and the source term as follows

$$\mathbf{u}_0(\mathbf{x}) = \nabla\varphi^e_{P,0}(\mathbf{x}) + \mathbf{curl}\,\varphi^e_{S,0}(\mathbf{x}), \qquad \mathbf{z}_0(\mathbf{x}) = \nabla\bar{\varphi}^e_{P,0}(\mathbf{x}) + \mathbf{curl}\,\bar{\varphi}^e_{S,0}(\mathbf{x})$$

$$\mathbf{g}(\mathbf{x},t) = \nabla \mathrm{g}_P(\mathbf{x},t) + \mathbf{curl}\,\mathrm{g}_S(\mathbf{x},t), \qquad \mathbf{f}(\mathbf{x},t) = \nabla \mathrm{f}_P(\mathbf{x},t) + \mathbf{curl}\,\mathrm{f}_S(\mathbf{x},t) \tag{34}$$

we obtain that the exterior elastodynamics problem (1) is formally equivalent (see [2]) to the following exterior potentials problem:

$$\begin{cases} \dfrac{\partial^2\varphi^e_P}{\partial t^2} - v_P^2\nabla^2\varphi^e_P = \dfrac{1}{\rho}\mathrm{f}_P & (\mathbf{x},t) \in \Omega^e \times (0,T] \\ \dfrac{\partial^2\varphi^e_S}{\partial t^2} - v_S^2\nabla^2\varphi^e_S = \dfrac{1}{\rho}\mathrm{f}_S & (\mathbf{x},t) \in \Omega^e \times (0,T] \\ \dfrac{\partial\varphi^e_P}{\partial\mathbf{n}_\Gamma} = \dfrac{\partial\varphi^e_S}{\partial\boldsymbol{\tau}_\Gamma} + \mathbf{g}\cdot\mathbf{n}_\Gamma =: \dfrac{\partial\varphi^e_S}{\partial\boldsymbol{\tau}_\Gamma} + g_{\mathbf{n}_\Gamma} & (\mathbf{x},t) \in \Gamma \times (0,T] \\ \dfrac{\partial\varphi^e_S}{\partial\mathbf{n}_\Gamma} = -\dfrac{\partial\varphi^e_P}{\partial\boldsymbol{\tau}_\Gamma} + \mathbf{g}\cdot\boldsymbol{\tau}_\Gamma =: -\dfrac{\partial\varphi^e_P}{\partial\boldsymbol{\tau}_\Gamma} + g_{\boldsymbol{\tau}_\Gamma} & (\mathbf{x},t) \in \Gamma \times (0,T] \\ \varphi^e_P(\mathbf{x},0) = \varphi^e_{P,0}(\mathbf{x}) & \mathbf{x} \in \Omega^e \\ \varphi^e_S(\mathbf{x},0) = \varphi^e_{S,0}(\mathbf{x}) & \mathbf{x} \in \Omega^e \\ \dfrac{\partial\varphi^e_P}{\partial t}(\mathbf{x},0) = \bar{\varphi}^e_{P,0}(\mathbf{x}) & \mathbf{x} \in \Omega^e \\ \dfrac{\partial\varphi^e_S}{\partial t}(\mathbf{x},0) = \bar{\varphi}^e_{S,0}(\mathbf{x}) & \mathbf{x} \in \Omega^e. \end{cases} \tag{35}$$

Moreover, note that, if we consider the Helmholtz decomposition (34) of the datum $\mathbf{g}$, the functions $g_{\mathbf{n}_\Gamma}$ and $g_{\boldsymbol{\tau}_\Gamma}$ are given by

$$g_{\mathbf{n}_\Gamma}(\mathbf{x},t) = \frac{\partial \mathrm{g}_P}{\partial\mathbf{n}_\Gamma}(\mathbf{x},t) - \frac{\partial \mathrm{g}_S}{\partial\boldsymbol{\tau}_\Gamma}(\mathbf{x},t)$$

$$g_{\boldsymbol{\tau}_\Gamma}(\mathbf{x},t) = \frac{\partial \mathrm{g}_P}{\partial\boldsymbol{\tau}_\Gamma}(\mathbf{x},t) + \frac{\partial \mathrm{g}_S}{\partial\mathbf{n}_\Gamma}(\mathbf{x},t).$$

To determine the solution of (35) in the finite computational domain Ω, bounded externally by $\mathcal{B}$, we need to define on $\mathcal{B}\times[0,T]$ a couple of scalar TD-NRBCs. To this aim, we introduce the following well known single and double layer operators associated with the scalar $\star := P, S$-wave equation:

$$\begin{aligned} (\mathcal{V}_\star\psi)(\mathbf{x},t) &:= \int_0^t\int_\Gamma G_\star(\mathbf{x}-\mathbf{y},t-s)\psi(\mathbf{y},s)\,\mathrm{d}\Gamma_{\mathbf{y}}\mathrm{d}s \\ (\mathcal{K}_\star\lambda)(\mathbf{x},t) &:= \int_0^t\int_\Gamma G_{\mathbf{n}_\mathcal{D},\star}(\mathbf{x}-\mathbf{y},t-s)\lambda(\mathbf{y},s)\,\mathrm{d}\Gamma_{\mathbf{y}}\mathrm{d}s \end{aligned} \tag{36}$$

where the kernel function is

$$G_\star(\mathbf{x},t) := \frac{1}{2\pi}\frac{H\left(t-\dfrac{\|\mathbf{x}\|}{v_\star}\right)}{\sqrt{t^2-\dfrac{\|\mathbf{x}\|^2}{v_\star^2}}},$$

and we have set $G_{\mathbf{n}_\mathcal{D},\star} := \partial_{\mathbf{n}_\mathcal{D}} G_\star$. Hence, we define the following TD-NRBCs on $\mathcal{B}$:

$$\begin{cases} \frac{1}{2}\varphi_P^e(\mathbf{x},t) + (\mathcal{K}_P\varphi_P^e)(\mathbf{x},t) - (\mathcal{V}_P(\partial_{\mathbf{n}_\mathcal{D}}\varphi_P^e))(\mathbf{x},t) = I_{\varphi_{P,0}}(\mathbf{x},t) + I_{\bar{\varphi}_{P,0}}(\mathbf{x},t) + I_{\mathrm{f}_P}(\mathbf{x},t) \\ \frac{1}{2}\varphi_S^e(\mathbf{x},t) + (\mathcal{K}_S\varphi_S^e)(\mathbf{x},t) - (\mathcal{V}_S(\partial_{\mathbf{n}_\mathcal{D}}\varphi_S^e))(\mathbf{x},t) = I_{\varphi_{S,0}}(\mathbf{x},t) + I_{\bar{\varphi}_{S,0}}(\mathbf{x},t) + I_{\mathrm{f}_S}(\mathbf{x},t), \end{cases} \tag{37}$$

where

$$\begin{aligned} I_{\varphi_{\star,0}}(\mathbf{x},t) &:= \frac{1}{v_\star^2}\frac{\partial}{\partial t}\int_\mathcal{D} G_\star(\mathbf{x}-\mathbf{y},t)\varphi_{\star,0}^e(\mathbf{y},t)\mathrm{d}\mathbf{y} \\ I_{\bar{\varphi}_{\star,0}}(\mathbf{x},t) &:= \frac{1}{v_\star^2}\int_\mathcal{D} G_\star(\mathbf{x}-\mathbf{y},t)\bar{\varphi}_{\star,0}^e(\mathbf{y},t)\mathrm{d}\mathbf{y} \\ I_{\mathrm{f}_\star}(\mathbf{x},t) &:= \frac{1}{\rho v_\star^2}\int_0^t\int_\mathcal{D} G_\star(\mathbf{x}-\mathbf{y},t-s)\mathrm{f}_\star^e(\mathbf{y},s)\mathrm{d}\mathbf{y}\mathrm{d}s \end{aligned} \tag{38}$$

are the volume integrals associated with the initial data and the body force.

To restrict the original problem in the finite computational domain Ω, we impose the continuity transmission conditions of the P and S-waves as well as of their normal derivatives on the artificial boundary $\mathcal{B}$. As previously remarked, without loss of generality, we assume that the local supports of $\mathbf{u}_0$, $\mathbf{z}_0$ and $\mathbf{f}$ are contained in Ω, so that $I_{\varphi_{\star,0}} = I_{\bar{\varphi}_{\star,0}} = I_{\mathrm{f}_\star} = 0$.

Hence, denoting by φ_P and φ_S the restriction of the solutions φ_P^e and φ_S^e to Ω, we get:

$$\begin{cases} \frac{\partial^2\varphi_P}{\partial t^2}(\mathbf{x},t) - v_P^2\nabla^2\varphi_P(\mathbf{x},t) = \frac{1}{\rho}\mathrm{f}_P(\mathbf{x},t) & (\mathbf{x},t)\in\Omega\times(0,T] \\ \frac{\partial^2\varphi_S}{\partial t^2}(\mathbf{x},t) - v_S^2\nabla^2\varphi_S(\mathbf{x},t) = \frac{1}{\rho}\mathrm{f}_S(\mathbf{x},t) & (\mathbf{x},t)\in\Omega\times(0,T] \\ \frac{\partial\varphi_P}{\partial\mathbf{n}_\Gamma}(\mathbf{x},t) = \frac{\partial\varphi_S}{\partial\boldsymbol{\tau}_\Gamma}(\mathbf{x},t) + g_{\mathbf{n}\Gamma}(\mathbf{x},t) & (\mathbf{x},t)\in\Gamma\times(0,T] \\ \frac{\partial\varphi_S}{\partial\mathbf{n}_\Gamma}(\mathbf{x},t) = -\frac{\partial\varphi_P}{\partial\boldsymbol{\tau}_\Gamma}(\mathbf{x},t) + g_{\boldsymbol{\tau}\Gamma}(\mathbf{x},t) & (\mathbf{x},t)\in\Gamma\times(0,T] \\ \frac{1}{2}\varphi_P(\mathbf{x},t) + (\mathcal{K}_P\varphi_P)(\mathbf{x},t) + (\mathcal{V}_P(\partial_\mathbf{n}\varphi_P))(\mathbf{x},t) = 0, & (\mathbf{x},t)\in\mathcal{B}\times(0,T] \\ \frac{1}{2}\varphi_S(\mathbf{x},t) + (\mathcal{K}_S\varphi_S)(\mathbf{x},t) + (\mathcal{V}_S(\partial_\mathbf{n}\varphi_S))(\mathbf{x},t) = 0, & (\mathbf{x},t)\in\mathcal{B}\times(0,T]. \end{cases} \tag{39}$$

2.2.1. Variational formulation of the PDE system in the interior domain

Proceeding analogously to the vectorial case, we consider the variational formulation for the wave equations, and the strong one for the TD-NRBCs.

To this aim, we introduce the spaces

$$V = H^1(\Omega), \qquad X = H^{-1/2}(\mathcal{B})$$

and, by abuse of notation with respect to that used in Section 2.1.1, the bilinear form

$$a(u,w) = \int_\Omega \nabla u(\mathbf{x})\cdot\nabla w(\mathbf{x})\mathrm{d}\mathbf{x},$$

the standard $L^2(\Omega)$ scalar product

$$(u,w)_\Omega = \int_\Omega u(\mathbf{x})w(\mathbf{x})\mathrm{d}\mathbf{x}$$

and the bilinear forms associated with the duality product

$$b_D(u,w) := \langle u, w\rangle_D, \qquad D = \Gamma, \mathcal{B}.$$

By taking into account the third and fourth relation in (39), the weak form of the first two equations of the novel problem is: for any $t \in (0,T]$, find $\varphi_P(t), \varphi_S(t) \in V$, $\lambda_P(t) := (\partial_{\mathbf{n}}\varphi_P)(t), \lambda_S(t) := (\partial_{\mathbf{n}}\varphi_S)(t) \in X$ such that

$$\begin{cases} \dfrac{d^2}{dt^2}(\varphi_P(t),\psi_P)_\Omega + v_P^2 a(\varphi_P(t),\psi_P) - v_P^2 b_\Gamma(\partial_{\boldsymbol{\tau}_\Gamma}\varphi_S(t),\psi_P) - v_P^2 b_{\mathcal{B}}(\lambda_P(t),\psi_P) \\ \qquad = \dfrac{1}{\rho}(\mathrm{f}_P(t),\psi_P)_\Omega + v_P^2(g_{\mathbf{n}_\Gamma}(t),\psi_P)_\Gamma \qquad \text{for all } \psi_P \in V \\ \dfrac{d^2}{dt^2}(\varphi_S(t),\psi_S)_\Omega + v_S^2 a(\varphi_S(t),\psi_S) + v_S^2 b_\Gamma(\partial_{\boldsymbol{\tau}_\Gamma}\varphi_P(t),\psi_S) - v_S^2 b_{\mathcal{B}}(\lambda_S(t),\psi_S) \\ \qquad = \dfrac{1}{\rho}(\mathrm{f}_S(t),\psi_S)_\Omega + v_S^2(g_{\boldsymbol{\tau}_\Gamma}(t),\psi_S)_\Gamma \qquad \text{for all } \psi_S \in V \\ \dfrac{1}{2}\varphi_P(t)(\mathbf{x}) + (\mathcal{K}_P\varphi_P)(t)(\mathbf{x}) + (\mathcal{V}_P(\lambda_P))(t)(\mathbf{x}) = 0 \qquad \mathbf{x} \in \mathcal{B} \\ \dfrac{1}{2}\varphi_S(t)(\mathbf{x}) + (\mathcal{K}_S\varphi_S)(t)(\mathbf{x}) + (\mathcal{V}_S(\lambda_S))(t)(\mathbf{x}) = 0 \qquad \mathbf{x} \in \mathcal{B}, \end{cases} \tag{40}$$

together with the associated initial conditions.

2.2.2. Discretization of the TD-NRBCs

Time discretization.. Proceeding as in Section 2.1.2, we approximate the time integrals in (36) by applying the Lubich convolution quadrature formula. Denoting by $\varphi_\star^n(\mathbf{y}) \approx \varphi_\star(t_n)(\mathbf{y})$ and $(\partial_{\mathbf{n}}\varphi_\star)^n(\mathbf{y}) \approx \partial_{\mathbf{n}}\varphi_\star(t_n)(\mathbf{y})$, for $\star = P, S$, we have

$$\begin{aligned} (\mathcal{V}_\star(\partial_{\mathbf{n}}\varphi_\star))(\mathbf{x},t_n) &\approx \sum_{j=0}^{n}\int_{\mathcal{B}} \omega_{n-j}(\Delta_t;\widehat{G}_\star(r))\,(\partial_{\mathbf{n}}\varphi_\star)^j(\mathbf{y})\,\mathrm{d}\mathcal{B}_{\mathbf{y}} \\ (\mathcal{K}_\star\varphi_\star)(\mathbf{x},t_n) &\approx \sum_{j=0}^{n}\int_{\mathcal{B}} \omega_{n-j}(\Delta_t;\widehat{G}_{\mathbf{n}_\mathcal{D},\star}(r))\,\varphi_\star^j(\mathbf{y})\,\mathrm{d}\mathcal{B}_{\mathbf{y}}, \end{aligned} \tag{41}$$

where $r = \|\mathbf{x}-\mathbf{y}\|$. The coefficients $\omega_n(\Delta_t; W(r))$, whose expression is given by (9), are associated with the Laplace transforms of $W = G_\star, G_{\mathbf{n}_\mathcal{D},\star}$ and are then approximated by formula (10). The Laplace transforms of W in this case are defined by

$$\widehat{G}_\star(r,s) = \frac{1}{2\pi}K_0\left(\frac{rs}{v_\star}\right), \tag{42}$$

$$\widehat{G}_{\mathbf{n}_\mathcal{D},\star}(r,s) = -\frac{s}{2\pi}K_1\left(\frac{rs}{v_\star}\right)\frac{\partial r}{\partial \mathbf{n}_\mathcal{D}}, \tag{43}$$

where $K_0(z)$ and $K_1(z)$ are the second kind modified Bessel function of order 0 and 1, respectively. It is worth to point out that the above transforms are much simpler than the corresponding ones we have for the vector elastodynamics equation.

Space discretization.. Proceeding as in 2.1.2, we approximate the unknown functions $\varphi_\star^j(\mathbf{x})$ and $\lambda_\star^j(\mathbf{x}) := (\partial_{\mathbf{n}}\varphi_\star)^j(\mathbf{x})$, $\mathbf{x} \in \mathcal{B}$, by

$$\varphi_\star^j(\boldsymbol{\eta}(\vartheta)) \approx \sum_{k=1}^{M}\varphi_\star^{k,j}N_k(\vartheta), \quad \lambda_\star^j(\boldsymbol{\eta}(\vartheta)) \approx \sum_{k=1}^{M}\lambda_\star^{k,j}N_k(\vartheta), \tag{44}$$

N_k being the piece-wise linear basis functions associated with the partitioning of the parameterization interval $[0,1]$ (see (18)).

To apply a nodal collocation method, we insert (44) into the TD-NRBCs of (40) and we collocate the latter at the collocation points ϑ_m, $m = 1, \ldots, M$. The matrix form of the TD-NRBC then takes the form:

$$\begin{cases} \left(\frac{1}{2}\mathbf{I} + \mathbf{K}_P^0\right)\boldsymbol{\varphi}_P^{\mathcal{B},n} + \sum_{j=0}^{n-1} \mathbf{K}_P^{n-j}\boldsymbol{\varphi}_P^{\mathcal{B},j} + \mathbf{V}_P^0\boldsymbol{\lambda}_P^{\mathcal{B},n} + \sum_{j=0}^{n-1} \mathbf{V}_P^{n-j}\boldsymbol{\lambda}_P^{\mathcal{B},j} = \mathbf{0} \\ \left(\frac{1}{2}\mathbf{I} + \mathbf{K}_S^0\right)\boldsymbol{\varphi}_S^{\mathcal{B},n} + \sum_{j=0}^{n-1} \mathbf{K}_S^{n-j}\boldsymbol{\varphi}_S^{\mathcal{B},j} + \mathbf{V}_S^0\boldsymbol{\lambda}_S^{\mathcal{B},n} + \sum_{j=0}^{n-1} \mathbf{V}_S^{n-j}\boldsymbol{\lambda}_S^{\mathcal{B},j} = \mathbf{0} \end{cases} \tag{45}$$

in the unknowns $\boldsymbol{\varphi}_\star^{\mathcal{B},n} = (\varphi_\star^{1,n}, \ldots, \varphi_\star^{M,n})^T$ and $\boldsymbol{\lambda}_\star^{\mathcal{B},n} = (\lambda_\star^{1,n}, \ldots, \lambda_\star^{M,n})^T$. The matrix entries of $\mathbf{V}_\star^n$ and $\mathbf{K}_\star^n$ are given by (see [8] for details on their computation):

$$(\mathbf{V}_\star^n)_{m,k} := \frac{1}{2\pi}\frac{\varrho^{-n}}{L}\sum_{l=0}^{L-1}\left(\int_0^1 K_0\left(\frac{r_m(\vartheta)z_l}{v_\star}\right)N_k(\vartheta)\,\|\boldsymbol{\eta}'(\vartheta)\|\,\mathrm{d}\vartheta\right)\mathrm{e}^{-\frac{\imath n l 2\pi}{L}} \tag{46}$$

and

$$(\mathbf{K}_\star^n)_{m,k} := -\frac{1}{2\pi}\frac{\varrho^{-n}}{L}\sum_{l=0}^{L-1}\left(\int_0^1 sK_1\left(\frac{r_m(\vartheta)z_l}{v_\star}\right)\frac{\partial r(\vartheta)}{\partial \mathbf{n}_{\mathcal{D}}}N_k(\vartheta)\,\|\boldsymbol{\eta}'(\vartheta)\|\,\mathrm{d}\vartheta\right)\mathrm{e}^{-\frac{\imath n l 2\pi}{L}} \tag{47}$$

where $z_l := \gamma(\varrho \mathrm{e}^{\imath l 2\pi/L})/\Delta_t$ and $r_m(\vartheta) := \|\boldsymbol{\eta}(\vartheta_m) - \boldsymbol{\eta}(\vartheta)\|$.

From the computational point of view, assuming to know $\boldsymbol{\varphi}_\star^{\mathcal{B},j}$ and $\boldsymbol{\lambda}_\star^{\mathcal{B},j}$ at the time steps $j = 0, \cdots, n-1$, the couple of absorbing condition at time t_n is given by

$$\begin{cases} \left(\frac{1}{2}\mathbf{I} + \mathbf{K}_P^0\right)\boldsymbol{\varphi}_P^{\mathcal{B},n} + \mathbf{V}_P^0\boldsymbol{\lambda}_P^{\mathcal{B},n} = -\sum_{j=0}^{n-1} \mathbf{K}_P^{n-j}\boldsymbol{\varphi}_P^{\mathcal{B},j} - \sum_{j=0}^{n-1} \mathbf{V}_P^{n-j}\boldsymbol{\lambda}_P^{\mathcal{B},j} \\ \left(\frac{1}{2}\mathbf{I} + \mathbf{K}_S^0\right)\boldsymbol{\varphi}_S^{\mathcal{B},n} + \mathbf{V}_S^0\boldsymbol{\lambda}_S^{\mathcal{B},n} = -\sum_{j=0}^{n-1} \mathbf{K}_S^{n-j}\boldsymbol{\varphi}_S^{\mathcal{B},j} - \sum_{j=0}^{n-1} \mathbf{V}_S^{n-j}\boldsymbol{\lambda}_S^{\mathcal{B},j}. \end{cases} \tag{48}$$

In the next proposition, we show that when the boundary $\mathcal{B}$ is a circle of radius R, and the parametrization interval $[0,1]$ is subdivided into M equal parts of length h, all matrices (46), (47) turn out to be circulant. Note that in this case we have $\|\boldsymbol{\eta}'(\vartheta)\| = R$. Furthermore, to prove our statement we only need to consider the generic integral contained in the above matrix representations, that we denote by $a(m,k)$. For notational simplicity, in the proof we will also ignore the factor R.

Proposition 2.1. *When the boundary $\mathcal{B}$ is a circle of radius R, all matrices $\mathbf{V}_\star^n$, $\mathbf{K}_\star^n$ are circulant.*

Proof. We limit our proof to the matrices $\mathbf{V}_\star^n$, as the one for the matrices $\mathbf{K}_\star^n$ is very similar. Moreover, to simplify the notation, we set $\zeta_l^\star = \frac{z_l}{v_\star}$. Thus, to obtain our result, we need to examine the following integral:

$$a(m,k) := \int_0^1 K_0\left(\|\boldsymbol{\eta}(\vartheta) - \boldsymbol{\eta}(\vartheta_m)\|\zeta_l^\star\right)N_k(\vartheta)\,\mathrm{d}\vartheta.$$

We also need to consider the periodic extension of the parametrization function $\boldsymbol{\eta}(\vartheta)$, and recall the following obvious relation, which can be very easily demonstrated using well-known trigonometric identities:

$$\|\boldsymbol{\eta}(\theta+\alpha) - \boldsymbol{\eta}(\phi+\alpha)\| = \|\boldsymbol{\eta}(\theta) - \boldsymbol{\eta}(\phi)\|.$$

Next, we examine the elements

$$a(m,m+j)=\int_{\vartheta_{m+j-1}}^{\vartheta_{m+j+1}} K_0\left(\|\boldsymbol{\eta}(\vartheta)-\boldsymbol{\eta}(\vartheta_m)\|\zeta_l^\star\right)\, N_{m+j}(\vartheta)\,\mathrm{d}\vartheta,\quad m=1,\cdots,M,\, j=0,\cdots,M-m.$$

$$a(m,m-j)=\int_{\vartheta_{m-j-1}}^{\vartheta_{m-j+1}} K_0\left(\|\boldsymbol{\eta}(\vartheta)-\boldsymbol{\eta}(\vartheta_m)\|\zeta_l^\star\right)\, N_{m-j}(\vartheta)\,\mathrm{d}\vartheta,\quad m=1,\cdots,M,\, j=1,\cdots,m-1.$$

By introducing the linear change of variable $\vartheta=\phi+(m\pm j)h$, $\phi\in[-h,h]$, we obtain

$$\begin{aligned} a(m,m\pm j) &= \int_{-h}^{h} K_0\left(\|\boldsymbol{\eta}(\phi\pm(m+j)h)-\boldsymbol{\eta}(-jh\pm(m+j)h)\|\zeta_l^\star\right) N_0(\phi)\,\mathrm{d}\phi \\ &= \int_{-h}^{h} K_0\left(\|\boldsymbol{\eta}(\phi)-\boldsymbol{\eta}(\mp jh)\|\zeta_l^\star\right) N_0(\phi)\,\mathrm{d}\phi \end{aligned} \tag{49}$$

where $N_0(\phi)$ is the (hat) basis function defined on $[-h,h]$. Since $\mathcal{B}$ is a circle, taking into account the extension of its parametric representation we have $\boldsymbol{\eta}(-jh)=\boldsymbol{\eta}((M-j)h)$.

Using the latter identity, representation (49) can be rewritten in the following form, where $m=1,\cdots,M$:

$$a(m,m+j)=\int_{-h}^{h} K_0\left(\|\boldsymbol{\eta}(\phi)-\boldsymbol{\eta}((M-j)h)\|\zeta_l^\star\right) N_0(\phi)\,\mathrm{d}\phi =: a_{M-j}(h),\, j=0,\cdots,M-m$$

$$a(m,m-j)=\int_{-h}^{h} K_0\left(\|\boldsymbol{\eta}(\phi)-\boldsymbol{\eta}(jh)\|\zeta_l^\star\right) N_0(\phi)\,\mathrm{d}\phi =: a_{j}(h),\, j=1,\cdots,m-1.$$

From these, the proposition statement then follows. □

The major consequence of this result is that only the first row of each matrix must be computed; a great computational saving.

2.2.3. Discretization of the interior scalar PDE equations

Time discretization. As for the previous approach, for the time discretization we apply the Crank-Nicolson method. To this aim we introduce the new unknowns $z_P:=\frac{\partial\varphi_P}{\partial t}$ and $z_S:=\frac{\partial\varphi_S}{\partial t}$ and, proceeding as we did in Section 2.1.3, we obtain

$$\begin{cases} (\varphi_P^{n+1},\psi_P)_\Omega+\alpha v_P^2 a(\varphi_P^{n+1},\psi_P)-\alpha v_P^2 b_\Gamma(\partial_{\boldsymbol{\tau}_\Gamma}\varphi_S^{n+1},\psi_P)-\alpha v_P^2 b_{\mathcal{B}}(\lambda_P^{n+1},\psi_P)= \\ \quad (\varphi_P^{n},\psi_P)_\Omega-\alpha v_P^2 a(\varphi_P^{n},\psi_P)+\alpha v_P^2 b_\Gamma(\partial_{\boldsymbol{\tau}_\Gamma}\varphi_S^{n},\psi_P)+\alpha v_P^2 b_{\mathcal{B}}(\lambda_P^{n},\psi_P)+\Delta_t\,(z_P^n,\psi_P)_\Omega \\ \quad +\dfrac{\alpha}{\rho}(\mathrm{f}_P^{n+1}+\mathrm{f}_P^{n},\psi_P)_\Omega+\alpha v_P^2(g_{\mathbf{n}\Gamma}^{n+1}+g_{\mathbf{n}\Gamma}^{n},\psi_P)_\Gamma \qquad \text{for all}\,\psi_P\in V \\ (\varphi_S^{n+1},\psi_S)_\Omega+\alpha v_S^2 a(\varphi_S^{n+1},\psi_S)+\alpha v_S^2 b_\Gamma(\partial_{\boldsymbol{\tau}_\Gamma}\varphi_P^{n+1},\psi_S)-\alpha v_S^2 b_{\mathcal{B}}(\lambda_S^{n+1},\psi_S)= \\ \quad (\varphi_S^{n},\psi_S)_\Omega-\alpha v_S^2 a(\varphi_S^{n},\psi_S)-\alpha v_S^2 b_\Gamma(\partial_{\boldsymbol{\tau}_\Gamma}\varphi_P^{n},\psi_S)+\alpha v_S^2 b_{\mathcal{B}}(\lambda_S^{n},\psi_S)+\Delta_t\,(z_S^n,\psi_S)_\Omega \\ \quad +\dfrac{\alpha}{\rho}(\mathrm{f}_S^{n+1}+\mathrm{f}_S^{n},\psi_S)_\Omega+\alpha v_S^2(g_{\boldsymbol{\tau}\Gamma}^{n+1}+g_{\boldsymbol{\tau}\Gamma}^{n},\psi_S)_\Gamma \qquad \text{for all}\,\psi_S\in V. \end{cases} \tag{50}$$

together with

$$z_\star^{n+1}=\frac{2}{\Delta_t}(\varphi_\star^{n+1}-\varphi_\star^{n})-z_\star^{n}. \tag{51}$$

Space discretization. Let us define the finite element space V_h associated with the conforming triangulation of Ω introduced in Section 2.1.3

$$V_h=\{v_h\in C^0(\Omega): v_{h_{|K}}\in\mathbb{P}^1(K), K\in\mathcal{T}_h,\}\subset V,$$

whose basis functions $\{N_i^\Omega\}_{i\in\mathcal{S}}$ have been previously defined. It is worth noting that, contrarily to the standard approach, for which we directly impose the Dirichlet boundary condition on Γ, thus eliminating the degrees of freedom on it, in this case the values of φ_P and φ_S are not known on Γ. By abuse of notation, we use the same symbol $\mathcal{S}$ to denote here the full set of nodes of the triangular decomposition, that includes also those lying on Γ.

Further, we denote by X_h the space of continuous piece-wise linear functions defined on the boundary $\mathcal{B}$ by the finite element basis $\{N_i^\mathcal{B} = N_i^\Omega{}_{|_\mathcal{B}}\}_{i=1}^M$, recalling that M denotes the number of mesh-points inherited on $\mathcal{B}$ by the decomposition of Ω.

Introducing the vectors

$$\boldsymbol{\varphi}_\star^n = \left[\varphi_\star^{1,n}, \varphi_\star^{2,n}, \cdots, \varphi_\star^{S,n}\right]^T \quad \text{and} \quad \boldsymbol{\lambda}_\star^n = \left[\lambda_\star^{1,n}, \lambda_\star^{2,n}, \cdots, \lambda_\star^{M,n}\right]^T$$

of the unknown nodal values of $\varphi_\star^n(\mathbf{x})$ and $\lambda_\star^n(\mathbf{x})$ associated with the nodes of the triangular mesh, we consider the finite element approximations

$$\varphi_{\star,h}^n(\mathbf{x}) = \sum_{i=1}^S \varphi_\star^{i,n} N_i^\Omega(\mathbf{x}), \quad \lambda_{\star,h}^n(\mathbf{x}) = \sum_{i=1}^M \lambda_\star^{i,n} N_i^\mathcal{B}(\mathbf{x}) \quad \text{and} \quad (\partial_{\boldsymbol{\tau}_\Gamma}\varphi_{\star,h})^n(\mathbf{x}) = \sum_{i=1}^S \varphi_\star^{i,n}(\partial_{\boldsymbol{\tau}_\Gamma} N_i^\Omega)(\mathbf{x}).$$

Then, the matrix form of the discrete Galerkin scheme associated with (50), is

$$\begin{cases} (\mathbf{M} + \alpha v_P^2 \mathbf{A})\boldsymbol{\varphi}_P^{n+1} - \alpha v_P^2 \mathbf{B}\boldsymbol{\varphi}_S^{n+1} - \alpha v_P^2 \mathbf{Q}\boldsymbol{\lambda}_P^{n+1} = (\mathbf{M} - \alpha v_P^2 \mathbf{A})\boldsymbol{\varphi}_P^n + \alpha v_P^2 \mathbf{B}\boldsymbol{\varphi}_S^n + \alpha v_P^2 \mathbf{Q}\boldsymbol{\lambda}_P^n \\ \qquad + \Delta_t \mathbf{M}\mathbf{z}_P^n + \dfrac{\alpha}{\rho}\mathbf{f}_P^n + \alpha v_P^2 \mathbf{g}_{\mathbf{n}_\Gamma}^n \\ (\mathbf{M} + \alpha v_S^2 \mathbf{A})\boldsymbol{\varphi}_S^{n+1} + \alpha v_S^2 \mathbf{B}\boldsymbol{\varphi}_P^{n+1} - \alpha v_S^2 \mathbf{Q}\boldsymbol{\lambda}_S^{n+1} = (\mathbf{M} - \alpha v_S^2 \mathbf{A})\boldsymbol{\varphi}_S^n - \alpha v_S^2 \mathbf{B}\boldsymbol{\varphi}_P^n + \alpha v_S^2 \mathbf{Q}\boldsymbol{\lambda}_S^n \\ \qquad + \Delta_t \mathbf{M}\mathbf{z}_S^n + \dfrac{\alpha}{\rho}\mathbf{f}_S^n + \alpha v_S^2 \mathbf{g}_{\boldsymbol{\tau}_\Gamma}^n, \end{cases} \tag{52}$$

where the mass, stiffness and boundary matrices are defined, by abuse of notation with respect to that of the previous approach, by

$$\mathbf{M}_{ij} = \left(N_i^\Omega, N_j^\Omega\right)_\Omega, \quad \mathbf{A}_{ij} = a(N_i^\Omega, N_j^\Omega), \quad i,j = 1,\cdots,S,$$

$$\mathbf{Q}_{ij} = \int_\mathcal{B} N_i^\Omega(\mathbf{x}) N_j^\mathcal{B}(\mathbf{x})\mathrm{d}\mathcal{B}, \quad i = 1,\cdots,S,\ j = 1,\cdots,M,$$

$$\mathbf{B}_{ij} = \int_\Gamma N_i^\Omega(\mathbf{x})(\partial_{\boldsymbol{\tau}_\Gamma} N_j^\Omega)(\mathbf{x})\mathrm{d}\Gamma, \quad i,j = 1,\cdots,S.$$

The terms $\mathbf{f}_\star^n$ and $\mathbf{g}_\square^n$ in (52) are the column vectors whose j-th component, $j = 1,\cdots,S$, are defined by

$$\mathbf{f}_{\star,j}^n = (f_\star^{n+1} + f_\star^n, N_j^\Omega)_\Omega, \qquad \star = P, S,$$

and

$$\mathbf{g}_{\square,j}^n = (g_\square^{n+1} + g_\square^n, N_j^\Omega)_\Gamma, \quad \square = \boldsymbol{\tau}_\Gamma, \mathbf{n}_\Gamma.$$

Combining (52) with (48), and in accordance with the splitting $\mathcal{S} = \mathcal{S}^I \cup \mathcal{S}^\mathcal{B}$ of the set of the degrees of freedom (recall that, in this case, I includes also the nodes lying on Γ), we get the

following block partitioned linear system (with obvious meaning of the notation):

$$\begin{bmatrix} \mathbf{M}^{II}+\alpha_{_P}\mathbf{A}^{II} & \mathbf{M}^{I\mathcal{B}}+\alpha_{_P}\mathbf{A}^{I\mathcal{B}} & -\alpha_{_P}\mathbf{B}^{II} & \mathbf{O} & \mathbf{O} & \mathbf{O} \\ \mathbf{M}^{\mathcal{B}I}+\alpha_{_P}\mathbf{A}^{\mathcal{B}I} & \mathbf{M}^{\mathcal{B}\mathcal{B}}+\alpha_{_P}\mathbf{A}^{\mathcal{B}\mathcal{B}} & \mathbf{O} & \mathbf{O} & -\alpha_{_P}\mathbf{Q}^{\mathcal{B}\mathcal{B}} & \mathbf{O} \\ \alpha_{_S}\mathbf{B}^{II} & \mathbf{O} & \mathbf{M}^{II}+\alpha_{_S}\mathbf{A}^{II} & \mathbf{M}^{I\mathcal{B}}+\alpha_{_S}\mathbf{A}^{I\mathcal{B}} & \mathbf{O} & \mathbf{O} \\ \mathbf{O} & \mathbf{O} & \mathbf{M}^{\mathcal{B}I}+\alpha_{_S}\mathbf{A}^{\mathcal{B}I} & \mathbf{M}^{\mathcal{B}\mathcal{B}}+\alpha_{_S}\mathbf{A}^{\mathcal{B}\mathcal{B}} & \mathbf{O} & -\alpha_{_S}\mathbf{Q}^{\mathcal{B}\mathcal{B}} \\ \mathbf{O} & \frac{1}{2}\mathbf{I}+\mathbf{K}_P^0 & \mathbf{O} & \mathbf{O} & \mathbf{V}_P^0 & \mathbf{O} \\ \mathbf{O} & \mathbf{O} & \mathbf{O} & \frac{1}{2}\mathbf{I}+\mathbf{K}_S^0 & \mathbf{O} & \mathbf{V}_S^0 \end{bmatrix} \begin{bmatrix} \boldsymbol{\varphi}_P^{I,n+1} \\ \boldsymbol{\varphi}_P^{\mathcal{B},n+1} \\ \boldsymbol{\varphi}_S^{I,n+1} \\ \boldsymbol{\varphi}_S^{\mathcal{B},n+1} \\ \boldsymbol{\lambda}_P^{\mathcal{B},n+1} \\ \boldsymbol{\lambda}_S^{\mathcal{B},n+1} \end{bmatrix}$$

$$= \begin{bmatrix} \sum_{*=I}^{\mathcal{B}}(\mathbf{M}^{I*}-\alpha_{_P}\mathbf{A}^{I*})\boldsymbol{\varphi}_P^{*,n}+\alpha_{_P}\mathbf{B}^{II}\boldsymbol{\varphi}_S^{I,n}+\Delta_t\sum_{*=I}^{\mathcal{B}}\mathbf{M}^{I*}\mathbf{z}_P^{*,n}+\frac{\alpha}{\rho}\mathbf{f}_P^{I,n}+\alpha_{_P}\mathbf{g}_{\mathbf{n}_\Gamma}^{I,n} \\ \sum_{*=I}^{\mathcal{B}}(\mathbf{M}^{\mathcal{B}*}-\alpha_{_P}\mathbf{A}^{I*})\boldsymbol{\varphi}_P^{*,n}+\alpha_{_P}\mathbf{Q}^{\mathcal{B}\mathcal{B}}\boldsymbol{\lambda}_P^{\mathcal{B},n}+\Delta_t\sum_{*=I}^{\mathcal{B}}\mathbf{M}^{\mathcal{B}*}\mathbf{z}_P^{*,n}+\frac{\alpha}{\rho}\mathbf{f}_P^{\mathcal{B},n} \\ \sum_{*=I}^{\mathcal{B}}(\mathbf{M}^{I*}-\alpha_{_S}\mathbf{A}^{I*})\boldsymbol{\varphi}_S^{*,n}-\alpha_{_S}\mathbf{B}^{II}\boldsymbol{\varphi}_P^{I,n}+\Delta_t\sum_{*=I}^{\mathcal{B}}\mathbf{M}^{I*}\mathbf{z}_S^{*,n}+\frac{\alpha}{\rho}\mathbf{f}_S^{I,n}+\alpha_{_S}\mathbf{g}_{\boldsymbol{\tau}_\Gamma}^{I,n} \\ \sum_{*=I}^{\mathcal{B}}(\mathbf{M}^{\mathcal{B}*}-\alpha_{_S}\mathbf{A}^{I*})\boldsymbol{\varphi}_S^{*,n}+\alpha_{_S}\mathbf{Q}^{\mathcal{B}\mathcal{B}}\boldsymbol{\lambda}_S^{\mathcal{B},n}+\Delta_t\sum_{*=I}^{\mathcal{B}}\mathbf{M}^{\mathcal{B}*}\mathbf{z}_S^{*,n}+\frac{\alpha}{\rho}\mathbf{f}_S^{\mathcal{B},n} \\ -\sum_{j=0}^{n-1}\mathbf{K}_P^{n-j}\boldsymbol{\varphi}_{\mathcal{B},P}^{j}-\sum_{j=0}^{n-1}\mathbf{V}_P^{n-j}\boldsymbol{\lambda}_{\mathcal{B},P}^{j} \\ -\sum_{j=0}^{n-1}\mathbf{K}_S^{n-j}\boldsymbol{\varphi}_{\mathcal{B},S}^{j}-\sum_{j=0}^{n-1}\mathbf{V}_S^{n-j}\boldsymbol{\lambda}_{\mathcal{B},S}^{j} \end{bmatrix},$$

where we have set $\alpha_\star = \alpha v_\star^2$. We remark that, in the above system, we have taken into account the sparsity pattern of the involved matrices. In particular, it results that the sub-blocks $\mathbf{B}^{\mathcal{B}\mathcal{B}}$, $\mathbf{B}^{I\mathcal{B}}$ and $\mathbf{B}^{\mathcal{B}I}$ of $\mathbf{B}$ are null, as well as the sub-block $\mathbf{Q}^{I\mathcal{B}}$ of $\mathbf{Q}$.

Finally, the above system is combined with the following two relations that allows for updating the unknowns $\mathbf{z}_\star$, for $\star = P, S$:

$$\mathbf{z}_\star^{n+1} = \frac{2}{\Delta_t}(\boldsymbol{\varphi}_\star^{n+1}-\boldsymbol{\varphi}_\star^{n})-\mathbf{z}_\star^{n}. \tag{53}$$

3. Numerical results

In this section, the two approaches we have described in Sections 2.1 and 2.2 are tested, by applying them to three problems. In particular, we compare the new FEM-BEM scalar wave equation approach with that based on the standard vector formulation. Among the characterizing aspects of the two numerical approaches, in Example 1 we point out in particular that, despite the fact that both methods have been obtained by performing analogous discretizations, while the new one turns out to be unconditionally stable, the other one inherits the conditional stability

of the BEM scheme already highlighted in [8]. Moreover, in the case of the new approach, all the advantages regarding the computation of the BEM matrices involved in the discretized TD-NRBCs, underlined in [8], hold also for the associated FEM-BEM coupling.

From now on, we refer to the numerical solution of Problem (1) obtained by the new scalar approach as $\mathbf{u}^{\text{new}} = (u_1^{\text{new}}, u_2^{\text{new}})$, and to the one obtained by the standard vector approach by $\mathbf{u}^{\text{std}} = (u_1^{\text{std}}, u_2^{\text{std}})$. We point out that in the first case the solution $\mathbf{u}^{\text{new}}$ of the original elastodynamic problem, must be reconstructed by means of the relation $\mathbf{u}^{\text{new}} = \nabla\boldsymbol{\varphi}_P + \operatorname{curl}\boldsymbol{\varphi}_S$ (see Section 2.2) which involves the (analytic) calculation of the partial derivatives of the numerical solutions defined in (44).

All the numerical computation has been performed by standard (i.e., sequential) Matlab® codes and, for what concerns the FEM method, we have used the Partial Differential Equation Toolbox.

Example 1. In this first example, we consider Problem (1) defined on the domain $\Omega^e = \{\mathbf{x} = (x_1, x_2) \in \mathbb{R}^2 : x_1^2 + x_2^2 > 1\}$, external to the unit disc with boundary Γ and centered at the origin of the axes, endowed with homogeneous initial data and null source $\mathbf{f}$. The Dirichlet datum is $\mathbf{g} = (\mathrm{g}_1, \mathrm{g}_2)$, where

$$\mathrm{g}_1(\mathbf{x}, t) = t^3 \mathrm{e}^{-2t} \mathrm{e}^{-(x_1^2 + 2x_2^2)}, \qquad \mathrm{g}_2(\mathbf{x}, t) = t^3 \mathrm{e}^{-2t} \cos(x_1), \qquad \mathbf{x} \in \Gamma,\ t \in [0, T].$$

The chosen P, S-velocities are $v_P = \sqrt{3}$ and $v_S = 1$, the material density is $\rho = 1$ and the final time is $T = 1$.

We restrict the original problem to the finite computational domain Ω, bounded internally by Γ and externally by the circle of radius 2, i.e. $\mathcal{B} = \{\mathbf{x} = (x_1, x_2) : x_1^2 + x_2^2 = 4\}$.

In Figure 2 we report the 2D and 3D behaviour of the P and S-waves within the finite computational domain Ω at the final time instant. In Figure 3 we compare the behaviour of the solution $\mathbf{u} = (u_1, u_2)$ of the elastodynamic problem obtained by applying both approaches. As we can see, there is a good agreement between the solution of the two approaches. Finally, in Figure 4, the first three plots correspond to the solutions obtained by the new approach. In particular, from left to right, they represent the modulus of the P-wave displacement $\|\nabla\varphi_P\|$, the modulus of the S-wave displacement $\|\mathbf{curl}\,\varphi_S\|$ and the modulus of the total displacement $\|\mathbf{u}^{\text{new}}\| = \|\nabla\varphi_P + \mathbf{curl}\,\varphi_S\|$ at $t = T$. In the fourth plot we report the same quantity $\|\mathbf{u}^{\text{std}}\|$ obtained by the standard approach. Again, we highlight a very good accordance between the last two figures.

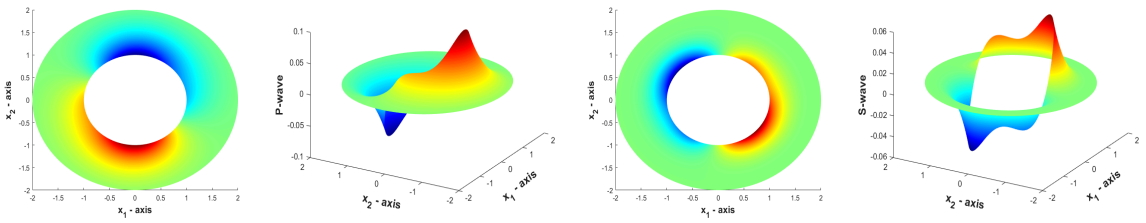

Figure 2: Example 1. Behaviour of φ_P (first two plots) and φ_S (last two plots) in Ω at $T = 1$.

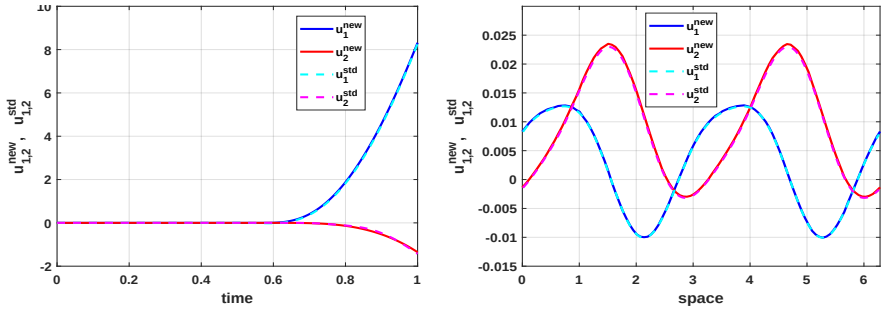

Figure 3: Example 1. Time-behaviour of $\mathbf{u}^*(\mathbf{x},t)$, $\mathbf{x}\approx(2,0)$ for $t\in[0,1]$ (left plot). Space-behaviour of $\mathbf{u}^*(\mathbf{x},T)$, for $T=1$ and $\mathbf{x}=\boldsymbol{\eta}(\vartheta)\in\mathcal{B}$, $\vartheta\in[0,2\pi]$ (right plot), $*=$ new, std.

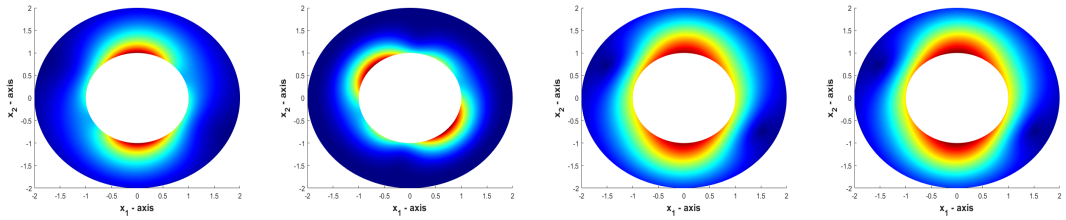

Figure 4: Example 1. Behaviour of P,S-waves in Ω. From left to right: $\|\nabla\varphi_P\|$, $\|\mathbf{curl}\,\varphi_S\|$, $\|\mathbf{u}^{\rm new}\|$ and $\|\mathbf{u}^{\rm std}\|$, at the final time instant $T=1$.

As remarked in [8], for the resolution of the elastodynamic problem by means of the mere collocation BEM method, to avoid the instability of the standard (vector) approach, the stepsizes Δ_t and h must satisfy the Courant-Friedrichs-Lewy (CFL) condition $\beta=v_P\Delta_t/h>0.17$. On the contrary, such limitation did not happen in the new (scalar) approach. In the FEM-BEM coupling method, it appears that the standard approach inherits the conditional stability of the associated collocation BEM, while the new one turns out to be unconditionally stable.

To show the above mentioned instability phenomenon, in Figure 5 (top row) we report the 3D plot of the solution $\|\mathbf{u}^{\rm std}\|$, obtained by applying the standard FEM-BEM approach with $h\approx 0.125$ and $N=104,106,116$. These values violate the CFL condition, β being slightly smaller than 0.17, and spurious oscillations soon appear on the artificial boundary $\mathcal{B}$, quickly exploding as N mildly increases. On the contrary, the new approach shows no instability (bottom row). After performing an extensive numerical testing the new approach showed no instability for various values of β definitely smaller than 0.17.

Furthermore, we remark that the vector field $\mathbf{u}^{\rm new}$ is retrieved from the P- and S-waves by computing their gradient and **curl**, respectively. Therefore the degree of accuracy, with respect to the space discretization, of the approximation of $\mathbf{u}^{\rm new}$ is lower than that associated with the computation of the P- and S-waves; a finer mesh is then needed to obtain a solution whose accuracy is similar to that produced by the vector method.

To show the accuracy of both methods, in Table 1 we report the relative errors $\mathrm{e}^*:=\|\mathbf{u}^{\rm ref}(\mathbf{x},t)-\mathbf{u}^*(\mathbf{x},t)\|/\|\mathbf{u}^{\rm ref}(\mathbf{x},t)\|$, $*=$ std, new, $\mathbf{u}^{\rm ref}(\mathbf{x},t)$ denoting the value of the reference solution at a fixed point $\mathbf{x}$ and $t=T$. The latter is obtained by applying a pure BEM with a very fine space-time discretization. In Table 1 the errors are computed by fixing the time step Δ_t and by refining the mesh. A refined triangular mesh is built based on a regular primal one, by subdividing each triangle into four new ones. The value of $\Delta_t=T/32$ has been chosen in such a way that, for all the three spacial refinements, the final errors are only affected by the mesh size parameter h. The initial values of h are chosen to guarantee a starting comparable accuracy of the two solutions

and have been successively halved in the standard approach and divided by four in the new one, to retrieve the expected quadratic and linear convergence order, respectively. It is worth to point out that, having applied two different Matlab solvers to the vector and scalar problems, slightly different initial meshes have been generated by the involved Matlab functions. Therefore, the errors are computed at two different but very close points. In particular, the reference point for the new approach is $\mathbf{x} = (2, 0)$, while for the standard one is $\mathbf{x} = (1.9995e + 00, 4.3629e - 02)$. Consequently, the reference values of the solutions are $\mathbf{u}^{\text{ref}}(\mathbf{x}, T) = (8.0934e - 03, -1.3827e - 03)$ and $\mathbf{u}^{\text{ref}}(\mathbf{x}, T) = (8.4015e - 03, -1.1511e - 03)$, respectively.

As we can notice, to assure the same accuracy as the standard approach, the new one requires a higher number n_T of mesh triangles and, therefore, the resolution of larger linear systems as well the computation of larger BEM matrices involved in them. For completeness, to compare the two approaches in terms of computational cost, in Table 1 we also report the corresponding values CPU, defined as the ratio between the total computational cost of the standard method and that of the new one. In the vector case, this is given by the computational cost required by the construction of the FEM and BEM matrices and the solution of the linear system to determine $\mathbf{u}^{\text{std}}$. In the new case, the cost of the post processing computation required to retrieve $\mathbf{u}^{\text{new}}$ has been added. Since all BEM matrices of the new approach are circulant (see Proposition 2.1) when $\mathcal{B}$ is a circle, we also report the CPU of the method, denoted by $CPU_{\mathcal{C}}$, which takes this property into account. It is worth noting that the computational cost of the new approach with respect to the standard one does not increase as fast as the size of the associated linear system does. This is mainly due to the fact that we need to construct, for each time instant, four BEM matrices for the new approach, and eight for the standard one.

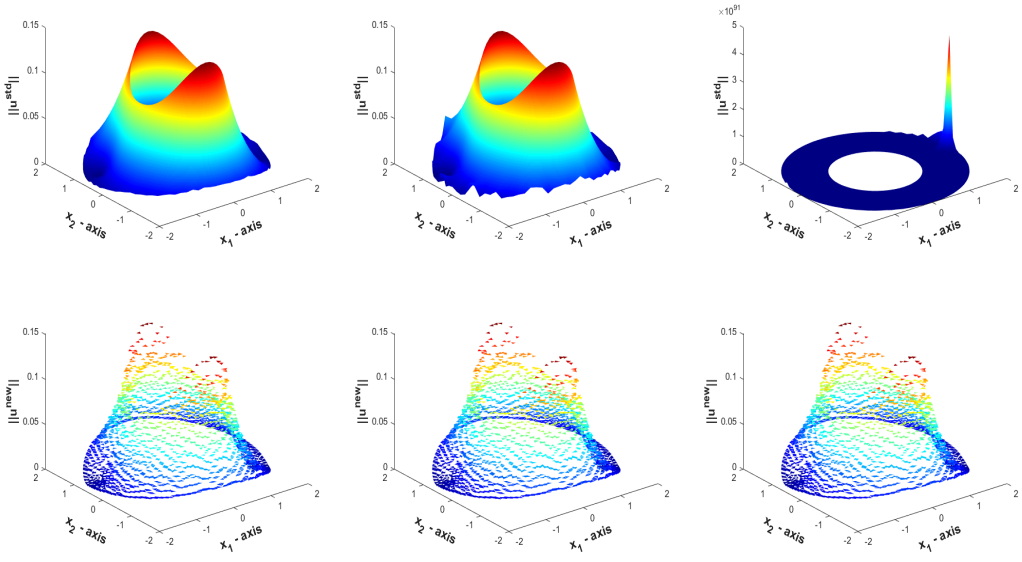

Figure 5: Example 1. The solutions $\|\mathbf{u}^{\text{std}}\|$ (top row) and $\|\mathbf{u}^{\text{new}}\|$ (bottom row) at the final time instant $T = 1$, for the choice $h \approx 0.125$ and, from left to right, $\Delta_t \approx 9.6e - 03, 9.4e - 03, 8.6e - 03$, respectively.

In the following examples, to compare the two approaches, the discretization parameters of the standard method are chosen such that its stability is guaranteed.

Example 2. In the same setting of Example 1, we consider an S-wave source term, localized in space, and defined in time by a Ricker pulse. In particular, referring to Problem (39), we choose

h	n_T	$\mathrm{e}^{\mathrm{std}}$	h	n_T	$\mathrm{e}^{\mathrm{new}}$	CPU	$CPU_{\mathcal{C}}$
$2.50e-01$	340	$2.34e-01$	$1.50e-01$	1450	$1.65e-01$	5.7	39
$1.25e-01$	1360	$7.66e-02$	$3.75e-02$	23200	$3.39e-02$	1.3	6.8
$6.25e-02$	5440	$1.62e-02$	$9.38e-03$	371200	$5.92e-03$	0.04	0.2

Table 1: Example 1. Errors e^{std} and e^{new}, and associated CPU.

a null source f_P and $\mathrm{f}_S(\mathbf{x},t) = h_S(x_1,x_2)r(t)$, with

$$h_S(x_1,x_2) = e^{-40((x_1-1.5)^2+x_2^2)} \quad \text{and} \quad r(t) = -18\pi^2 e^{-\pi^2(t-1)^2}(1-2\pi^2(t-1)^2), \quad t\in[0,4].$$

The initial data and $\mathbf{g}$ are null. The corresponding source for the solution $\mathbf{u}$ of Problem (6) is

$$\mathbf{f}(\mathbf{x},t) = r(t)\begin{bmatrix} \partial_{x_1} h_S(x_1,x_2) \\ -\partial_{x_2} h_S(x_1,x_2) \end{bmatrix}.$$

Since h_S decays exponentially fast away from its centre $\mathbf{x} = (1.5,0)$, the source f_S is regarded as compactly supported from the computational point of view, and since the support is included in Ω, its contribution in the discrete scheme (50) appears in the right hand side vector $\mathbf{f}_S$. Analogously, for the standard approach, since both f_1 and f_2 can be considered computationally supported in Ω, the corresponding vectors $\mathbb{F}_1^n$ and $\mathbb{F}_2^n$ in the right hand side of the final linear system are the non null terms involved in the time marching Crank Nicolson scheme at the time instant t_n.

In Figure 6 we report the 2D and 3D behaviour of the P- and S-waves within the finite computational domain Ω at the time instants $t = 1$ and $t = 2$.

In Figure 7 we present the snapshots of the numerical solution obtained at the fixed time instants $t_n = 0.75, 1.25, 1.75, 2, 2.5, 4$. The first three columns represent the solution obtained by the new FEM-BEM method ($\|\nabla\varphi_P\|$, $\|\mathbf{curl}\,\varphi_S\|$ and $\|\mathbf{u}^{\mathrm{new}}\|$, respectively) while the last one refers to the solution $\|\mathbf{u}^{\mathrm{std}}\|$. As we can see, there is a very good agreement between the last two columns.

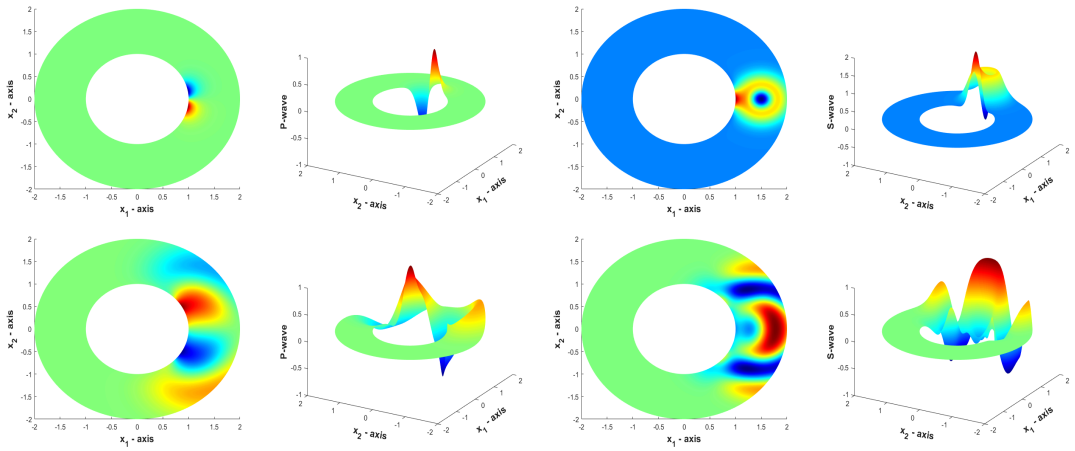

Figure 6: Example 2. Behaviour of φ_P (first two columns) and φ_S (last two columns) in Ω at the time instants $t = 1$ (top row) and $t = 2$ (bottom row).

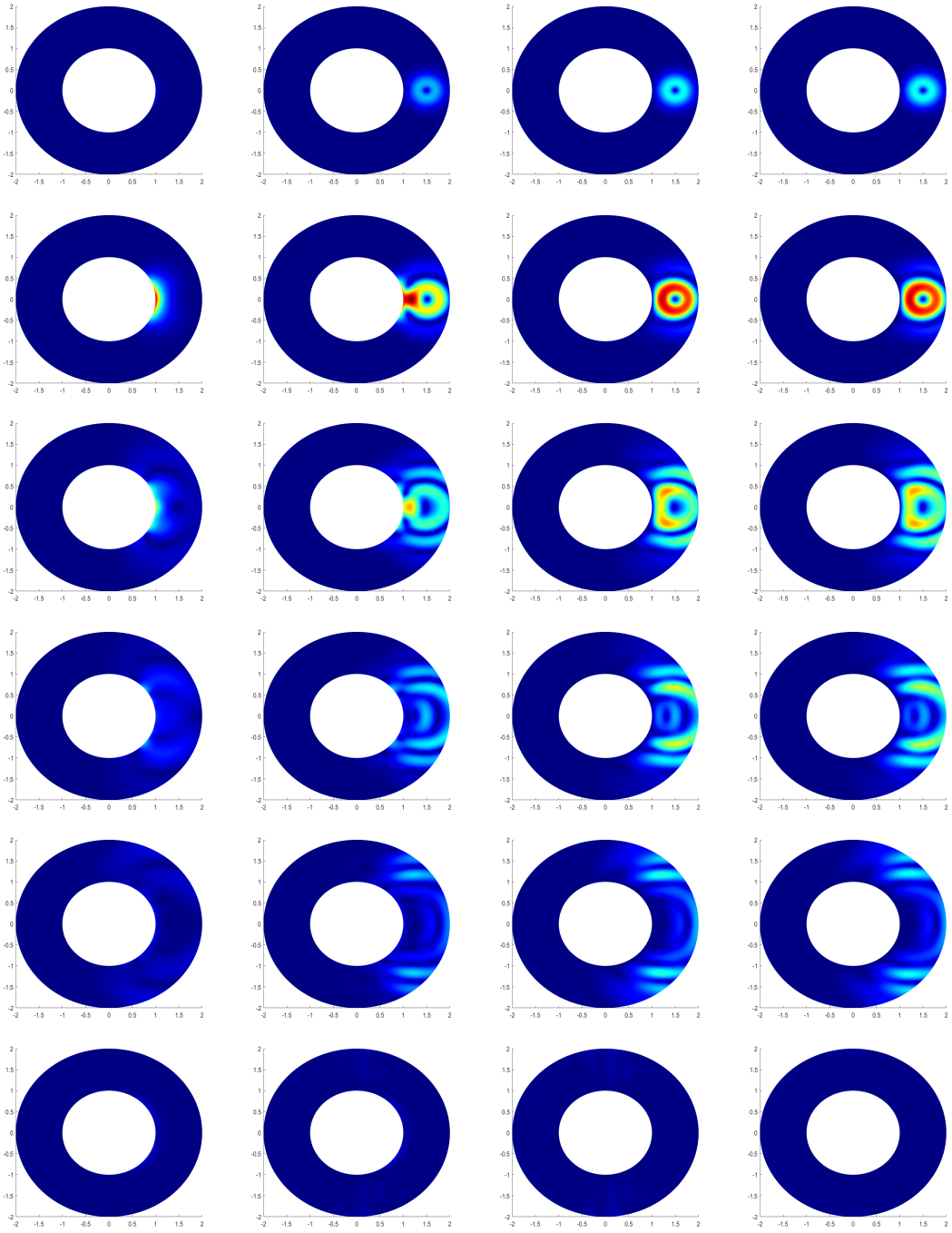

Figure 7: Example 2. Behaviour of P, S-waves in Ω at different time instants. From left to right columns: $\|\nabla\varphi_P\|$, $\|\mathbf{curl}\,\varphi_S\|$, $\|\mathbf{u}^{\mathrm{new}}\|$ and $\|\mathbf{u}^{\mathrm{std}}\|$.

Example 3. In this final example, we aim at simulating situations where one is interested in knowing the solution at points that are away from sources. We assume that the initial conditions and the Dirichlet datum are null, and we study the propagation of elastic waves generated by a source $\mathbf{f}$ located away from the obstacle. In such a case, to avoid the choice of a large computation domain including the support of $\mathbf{f}$ and, consequently, the waste of computational time and space memory, it is convenient to choose the artificial boundary $\mathcal{B}$ in such a way that the source is locally

supported in the residual domain $\mathcal{D}$. Therefore, a suitable modification of the TD-NRBC is needed. This consists in adding the extra "volume" integral terms in Equations (3) and (37) for the standard vector and the new scalar approaches, respectively. For the details on the computation of these latter, we refer to Example 3 in [8].

In particular, we consider the unit disc as physical obstacle, $\mathrm{f}_P = 0$ and the locally supported $\mathrm{f}_S(\mathbf{x}, t) = h_S(x_1, x_2)r(t)$, with

$$h_S(x_1, x_2) = e^{-40((x_1-2.5)^2+x_2^2)} \quad \text{and} \quad r(t) = t^3 e^{-t}\sin(2t), \quad t \in [0, 8].$$

To show that both approaches allow to treat external sources, we apply them in two different geometrical settings: the artificial boundary, in the first case, is the circumference of radius 1.5, in the second one, the ellipse with horizontal and vertical semi-axis 3.5 and 1.5, respectively. Therefore the source term f_S is located outside the computational domain in the former case, inside in the latter one.

In Figure 8 we show the behaviour of $\mathbf{u}^{\mathrm{new}}$ obtained by the new scalar approach at the time instants $t_n = 2, 3, 4, 4.5, 5.5, 6, 7, 7.5$ (proceeding row by row, from top-left to bottom-right). For each instant we represent the numerical solution associated with both choices of the computational domain. As we can see, the solutions reported in the first and third columns perfectly match with the restriction to the circular annulus of those represented in the second and fourth columns. Very similar results have been obtained by the standard vector approach, and we omit them for brevity.

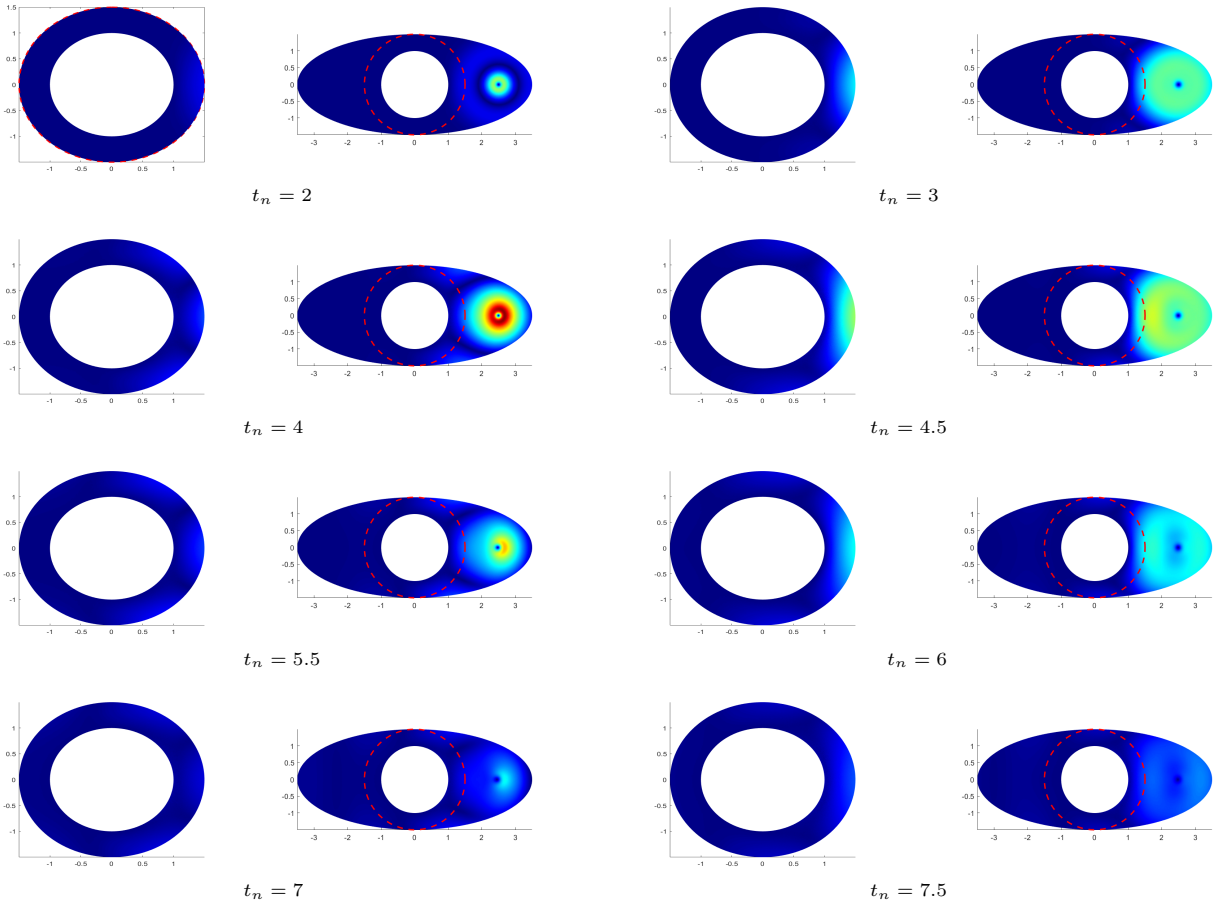

Figure 8: Example 3. Behaviour of $\mathbf{u}^{\mathrm{new}}$ at different time instants for two types of artificial boundary.

4. Conclusions

We have compared two numerical methods for the resolution of 2D exterior elastodynamic problems with Dirichlet boundary conditions, both based on a FEM-BEM coupling. The first method is the classical one, derived from the vector formulation of the problem; the second is a novel approach, obtained by reformulating the original PDE in terms of two coupled scalar wave equations involving, as new unknowns, the P (primary) and S (secondary) waves. The novel approach is of particular interest when the problem source is a P-wave or a S-wave, and the knowledge of the propagation of the waves generated by this source is required. We highlight here the main pros and cons of the two methods, resulting from a numerical comparison of their significant "ingredients".

- In both cases, the major issue is the efficient evaluation of the integral operators involved in the definition of the boundary integral non-reflecting condition. In this regard, the simple expression of the Laplace transformed kernels for the scalar approach, compared to those of the vector one, represents the most significant advantage of the new method. Indeed, as remarked in [8], the efficient evaluation of the vector kernels requires special procedures, so that the computation of the matrix entries in the novel approach is much faster.

- A further advantage of the new scalar method, that allows us to speed up significantly the computation and to save memory space, confirmed by Proposition 2.1, is the circulant structure of all the BEM matrices when the artificial boundary $\mathcal{B}$ is a circle, uniformly partitioned. A case of interest when this choice is consistent with the geometry of the physical obstacle. The standard approach does not benefit of this advantage.

- The novel approach requires the post processing computation of the partial derivatives of the P- and S-waves to retrieve the solution $\mathbf{u}$ of the original problem. This step does not represent a drawback, since it has a negligible cost with respect to that of the global scheme. However, it is important to point out that, since the degree of accuracy of the approximation of $\mathbf{u}$ is lower than that associated with the P- and S-waves, a finer mesh is needed to obtain a solution whose accuracy is similar to that produced by the vector method. So this implies that the scalar method must also be applied with this finer mesh.

- A common drawback of both methods is the recalculation, at each time step, of all the matrix-vector products in each sum on the right-hand side of the equations defining the non-reflecting boundary condition. In fact, the updating of these terms requires a higher cost the finer is the inherited mesh on $\mathcal{B}$. To overcome this, a possible remedy could be the use of special sparsification strategies of the BEM matrices, a task that has already been examined in the context of scalar wave propagation (see [1, 4]); but this requires further investigations, in particular for the vector approach.

- Finally, from an extensive numerical testing, it appears that the novel approach is unconditionally stable, while in the vector approach a CFL condition must be satisfied by the space-time discretization steps. The latter represents one of the most important advantages we have found, especially when one has to retrieve highly oscillating solutions over time or solutions defined in complex geometries.

Acknowledgments

The authors are grateful to the referees for their helpful and constructive comments.

The present research has been performed in the framework of MIUR grant *"Dipartimenti di Eccellenza 2018-2022"*, CUP E11G18000350001, and supported by the GNCS-INdAM 2020 research program *"Metodologie innovative per problemi di propagazione di onde in domini illimitati: aspetti teorici e computazionali"*.

References

[1] S. Bertoluzza, S. Falletta, and L. Scuderi. Wavelets and convolution quadrature for the efficient solution of a 2D space-time BIE for the wave equation. *Applied Mathematics and Computation*, 366:124726, 2020.

[2] A. Burel, S. Impériale, and P. Joly. Solving the homogeneous isotropic linear elastodynamics equations using potentials and finite elements. The case of the rigid boundary condition. *Numer. Analys. Appl.*, 5(2):136–143, 2012.

[3] T.A Cruse and F.J. Rizzo. A direct formulation and numerical solution of the general transient elastodynamic problem. I. *J. Math. Anal. Appl.*, 22:244–259, 1968.

[4] L. Desiderio and S. Falletta. Efficient solution of 2D wave propagation problems by CQ-wavelet BEM: algorithm and applications. *SIAM Journal on Scientific Computing*, 42(4):B894–B920, 2020.

[5] A.C. Eringer and E.S. Suhubi. *Elastodynamics*, volume 2. Academic Press, New York, 1975.

[6] S. Falletta, G. Monegato, and L. Scuderi. A space-time BIE methods for nonhomogeneous exterior wave equation problems. The Dirichlet case. *IMA J. Numer. Anal.*, 32(1):202–226, 2012.

[7] S. Falletta, G. Monegato, and L. Scuderi. A space-time BIE method for wave equation problems: the (two-dimensional) Neumann case. *IMA J. Numer. Anal.*, 34(1):390–434, 2014.

[8] S. Falletta, G. Monegato, and L. Scuderi. Two boundary integral equation methods for linear elastodynamics problems on unbounded domains. *Computers and Mathematics with Applications*, 78(12):3841–3861, 2019.

[9] A. Furukawa, T. Saitoh, and S. Hirose. Convolution quadrature time-domain boundary element method for 2-D and 3-D elastodynamic analyses in general anisotropic elastic solids. *Eng. Anal. Bound. Elem.*, 39:64–74, 2014.

[10] I.S. Gradshteyn and I.M. Ryzhik. *Table of Integrals, Series, and Products*. Academic Press, New York, 2007.

[11] L. Kielhorn and M. Schanz. Convolution quadrature method-based symmetric Galerkin boundary element method for 3-D elastodynamics. *Int. J. Numer. Meth. Engng*, 76:1724–1746, 2008.

[12] C. Lubich. Convolution quadrature and discretized operational calculus. I. *Numer. Math.*, 52:129–145, 1988.

[13] C. Lubich. On the multistep time discretization of linear initial-boundary value problems and their boundary integral equations. *Numer. Math.*, 67(3):365–389, 1994.

[14] T. Maruyama, T. Saitoh, T.Q. Bui, and S. Hirose. Transient elastic wave analysis of 3-D large-scale cavities by fast multipole BEM using implicit Runge-Kutta convolution quadrature. *Comput. Methods Appl. Mech. Engrg.*, 303:231–259, 2016.

[15] C.C. Spyrakos and H. Antes. Time domain boundary element method approaches in elastodynamics: a comparative study. *Comput. Struct.*, 24:529–535, 1986.

[16] C.A.R. Vera-Tudela and J.C.F. Telles. 2D elastodynamic with boundary element method and the operational quadrature method. *Proceeding of COBEM 2005*, 18th International Congress of Mechanical Engineering, November 6–11 2005.

[17] C.C. Wang, H.C Wang, and G.S. Liou. Quadratic time domain BEM formulation for 2D elastodynamic transient analysis. *Int. J. Solids Structures*, 34(1):129–151, 1997.